SANDIA REPORT

SAND2000-1015
Unlimited Release
Printed April 2000

Computational Methods for Coupling Microstructural and Micromechanical Materials Response Simulations

Elizabeth A. Holm, Corbett C. Battaile, Thomas E. Buchheit, H. Eliot Fang, Mark D. Rintoul, Venkata Vedula, S. Jill Glass, Gerald A. Knorovsky, Michael K. Neilsen, Gerald W. Wellman, Deborah Sulsky, Yu-Lin Shen, and H. Buch Schreyer

Prepared by
Sandia National Laboratories
Albuquerque, New Mexico 87185 and Livermore, California 94550

Sandia is a multiprogram laboratory operated by Sandia Corporation, a Lockheed Martin Company, for the United States Department of Energy under Contract DE-AC04-94AL85000.

Sandia National Laboratories

Issued by Sandia National Laboratories, operated for the United States Department of Energy by Sandia Corporation.

Available to DOE and DOE contractors from
Office of Scientific and Technical Information
P.O. Box 62
Oak Ridge, TN 37831

Prices available from (703) 605-6000
Web site: http://www.ntis.gov/ordering.htm

Available to the public from
National Technical Information Service
U.S. Department of Commerce
5285 Port Royal Rd
Springfield, VA 22161

SAND2000-1015
Unlimited Release
Printed April 2000

Computational Methods for Coupling Microstructural and Micromechanical Materials Response Simulations

Elizabeth A. Holm and Corbett C. Battaile
Materials and Process Modeling and Computation

Thomas E. Buchheit
Mechanical Reliability and Melting

H. Eliot Fang and Mark D. Rintoul
Materials Simulation Sciences

Venkata Vedula, S. Jill Glass, and Gerald A. Knorovsky
Joining, Coating and Net Shaping

Michael K. Neilsen and Gerald W. Wellman
Thermal/Fluids Engineering
Sandia National Laboratories
P. O. Box 5800
Albuquerque, NM 87185-1411 USA

Prof. Deborah Sulsky, Prof. Yu-Lin Shen, and Prof. H. Buck Schreyer
University of New Mexico
Albuquerque, NM USA

Abstract

Computational materials simulations have traditionally focused on individual phenomena: grain growth, crack propagation, plastic flow, etc. However, real materials behavior results from a complex interplay between phenomena. In this project, we explored methods for coupling mesoscale simulations of microstructural evolution and micromechanical response. In one case, massively parallel (MP) simulations for grain evolution and microcracking in alumina stronglink materials were dynamically coupled. In the other, codes for domain coarsening and plastic deformation in CuSil braze alloys were iteratively linked. This program provided the first comparison of two promising ways to integrate mesoscale computer codes. Coupled microstructural/micromechanical codes were applied to experimentally observed microstructures for the first time. In addition to the coupled codes, this project developed a suite of new computational capabilities (PARGRAIN, GLAD, OOF, MPM, polycrystal plasticity, front tracking). The problem of plasticity length scale in continuum calculations was recognized and a solution strategy was developed. The simulations were experimentally validated on stockpile materials.

Table of Contents

Introduction

Computational materials simulations have traditionally focused on an individual phenomenon: grain growth, crack propagation, plastic flow, etc. However, real materials behavior results from a complex interplay between phenomena. Linking computational models for coupled behavior mechanisms is a grand challenge in computational materials science.

Even general methodologies for linking simulation length and time scales have not been developed. In the broadest sense, we can delineate two extremes in simulation coupling. Computationally efficient codes for phenomena that occur on similar length and time scales may be dynamically coupled: both codes compute simultaneously on the same data set. Computationally intensive codes, or codes for phenomena which occur at greatly different length and time scales, must be iteratively linked: each code takes a turn evolving the system, then packages its output data in a form to be passed to the next code.

Utilizing model problems amenable to each of these approaches, we explored methods for coupling mesoscale (i.e. microstructural/micromechanical) simulations of materials behavior. In one case, massively parallel (MP) simulations for the physically coupled processes of grain evolution and microcracking in brittle materials were dynamically coupled. In the other, MP codes for domain coarsening and plastic deformation were iteratively linked. This program provided the first comparison of two promising ways to couple mesoscale computer codes.

The computer simulations were applied to problems in stockpile materials. Microcracking in brittle materials was studied in the context of alumina used in stronglinks. These materials are single phase, fracture is strictly brittle, and the ratio of inter- to transgranular fracture depends on processing. During the hot pressing process, anisotropic thermal expansion can cause microcracking along grain boundaries, which increases with grain size.

Plastic deformation studies focused on thermomechanical response of Ag-Cu (CuSil) braze alloys. During fabrication and service at high temperatures, grain growth can both mediate and be influenced by plastic deformation. This coupling can, in turn, lead to failure initiation.

In both materials systems, microstructural evolution occurs simultaneously with mechanical response. Diverse microstructural evolution models were implemented and their coupling characteristics were evaluated. These methods included a discrete Monte Carlo Potts Model (PARGRAIN), a continuum front-tracking model (FT), and a diffuse interface phase field model. Each was found useful in certain situations. In addition, we utilized OIM (Orientation Imaging Microscopy), an advanced experimental technique for characterizing microstructural geometry and crystallography, to provide real microstructures to the mechanics codes.

The problem of modeling the mechanics of brittle fracture is complicated by the stress singularity at the crack tip. To overcome the computational limitations of resolving

this singularity, we examined both a discrete ball and spring model (GLAD) and a continuum, finite element model with death elements (OOF).

Plastic flow was found to be amenable to a continuum approach. Both a conventional finite element model (JAS3D) as well as a meshless continuum model (MPM) were evaluated for their ability to accommodate microstructure and microstructural evolution.

In coupled microstructure/micromechanics codes, the microstructural evolution algorithm is used to form the initial microstructure. This grain configuration is mapped onto the mechanics model, setting local properties, and the first increment of the dynamic stress/strain field is applied. The mechanics model relaxes the system; the system deforms or fractures during this process. The resulting microstructure and local strain field are fed back to the microstructure model for further evolution. This alternating handshaking repeats until the simulation is complete.

The difference between the coupling methodologies for brittle fracture and plastic flow is the frequency of handshaking. In the brittle fracture code, both microstructural evolution and micromechanics codes are relatively efficient. They are coupled to act on the same data set, and a full mechanical relaxation is performed at every microstructural evolution timestep. Thus, this code is dynamically coupled. In the plastic flow code, direct coupling is not tractable even on the Teraflop machine. Instead, parametric accuracy studies determined the degree of change in the microstructure or mechanical state that requires re-evaluation by the other code, and the microstructural and micromechanical models are linked by an I/O interface. Thus, this code is iteratively linked.

Representative coupled codes were parallelized. Computational challenges to parallelization included timestep synchronization, mesh matching, and data passing.

Besides delivering coupled codes for microstructural and micromechanical response, this three-year project developed numerous new computational and experimental capabilities. In this report, we describe these efforts in detail, present results, and propose directions for future work.

Plastic deformation in CuSil braze alloys

Polycrystal plasticity model

Crystallographic slip and deformation twinning are the primary observed modes of plastic deformation at low homologous temperatures. Both modes of inelastic deformation take place exclusively on characteristic planes, i.e. slip planes or twinning planes, in characteristic directions, i.e. slip directions or twinning directions. The orientations of the characteristic planes and directions are a function of the geometry of the crystal. The microstructural mechanics model simulates the response of crystallographic slip in face centered cubic (FCC) metals, such as Copper, Aluminum and Nickel. The model can readily be extended to incorporate deformation by twinning or by

slip on different systems. In FCC crystals, the slip systems are defined using standard Miller index notation by $\langle 111 \rangle$ planes and $\{110\}$ directions. A total of 12 $\langle 111 \rangle \{110\}$ slip systems are defined in FCC crystals. Table I lists the slip systems as they are defined in the model implementation. Slip is bi-directional, resulting in 24 possible directions in which plastic deformation by slip in FCC crystals can occur.

Table I. FCC Slip Systems		
	Slip Plane	Slip Direction
1.	$\{11\bar{1}\}$	[011]
2.	$\{11\bar{1}\}$	[101]
3.	$\{11\bar{1}\}$	$[1\bar{1}0]$
4.	$\{1\bar{1}\bar{1}\}$	$[01\bar{1}]$
5.	$\{1\bar{1}\bar{1}\}$	[101]
6.	$\{1\bar{1}\bar{1}\}$	[110]
7.	$\{1\bar{1}1\}$	[011]
8.	$\{1\bar{1}1\}$	$[10\bar{1}]$
9.	$\{1\bar{1}1\}$	[110]
10.	{111}	$[01\bar{1}]$
11.	{111}	$[10\bar{1}]$
12.	{111}	$[1\bar{1}0]$

The microstructural mechanics model development implemented into JAS-3D finite element code parallels a kinematic framework with a basis originally proposed by Asaro and Rice [1] and Hill and Rice [2]. Researchers have used and presented this framework in slightly modified forms and have experimented with adding rate sensitivity, e.g. [3], and latent hardening, e.g. [4], to the model. More recently researchers have incorporated the constitutive model into FE code to simulate the deformation of metallic and ceramic single crystals and polycrystals, e.g. [5]. This same constitutive framework has recently been published in textbook form, in Chap. 8 and Tip. 11 of [6]. A detailed model development is given there, a summary of the model, emphasizing aspects of the JAS-3D implementation, is given in the following sub-sections.

Kinematic framework

Distortion of a continuum is described using the velocity gradient, which can be additively decomposed into symmetric and skew-symmetric parts as follows:

$$\mathbf{L} = \Omega + \mathbf{D} \tag{1}$$

where $\mathbf{D}$ is the symmetric deformation rate tensor and Ω is the skew-symmetric spin rate tensor. Distortion of single crystals has been described as a combination of plastic flow due to crystallographic slip and lattice distortion. Lattice distortion includes elastic distortion and rigid body rotation of the crystal lattice. Thus, for single crystals the deformation rate, $\mathbf{D}$, and spin rate, Ω, can be further decomposed into lattice and plastic parts as follows:

$$\mathbf{D} = \mathbf{D}_l + \mathbf{D}_p \tag{2a}$$

$$\Omega = \Omega_l + \Omega_p \tag{2b}$$

where $\mathbf{D}_l$ represents the lattice deformation rate, and $\mathbf{D}_p$ represents the plastic deformation rate due to crystallographic slip. Ω_l represents the lattice spin rate and Ω_p represents the plastic spin rate. The plastic deformation rate and spin rate depend on the slip rates, $\dot{\gamma}_s$, for the active slip systems,

$$\mathbf{D}_p = \sum_{s=1}^{12} \dot{\gamma}_s \mathbf{P}_s \tag{3}$$

$$\Omega_p = \sum_{s=1}^{12} \dot{\gamma}_s \mathbf{W}_s \tag{4}$$

$\mathbf{P}_s$ and $\mathbf{W}_s$ are the symmetric and skew-symmetric parts of the dyad, which is formed from the lattice vectors for each slip system, defined as:

$$\mathbf{P}_s = \frac{1}{2}(\mathbf{d}_s \otimes \mathbf{n}_s + \mathbf{n}_s \otimes \mathbf{d}_s) \tag{5}$$

$$\mathbf{W}_s = \frac{1}{2}(\mathbf{d}_s \otimes \mathbf{n}_s - \mathbf{n}_s \otimes \mathbf{d}_s) \tag{6}$$

where $\mathbf{d}_s$ represents a unit vector oriented in the slip direction for slip system s and $\mathbf{n}_s$ represents a unit vector normal to the slip plane for slip system s.

Based on the assumption that the elastic lattice properties are unaffected by slip, the constitutive relation given by [1] is as follows:

$$\overset{\nabla^*}{\sigma} + \sigma \, \mathrm{tr}(\mathbf{D}^*) = \boldsymbol{E} : \mathbf{D}^* \tag{7}$$

where $\overset{\nabla^*}{\sigma}$ is the co-rotational stress rate formed on axes which spin with the lattice, σ is the Cauchy stress, $\mathrm{tr}(\mathbf{D}^*)$ represents the trace of $\mathbf{D}^*$, in indicial notation D^*_{kk}, and $\boldsymbol{E}$ is the fourth order elasticity tensor. Anisotropic elastic response is included in the JAS-3D implementation of this model. Lattice vectors that characterize the slip systems are affected by lattice distortion. A variety of assumptions can be made concerning the evolution of the lattice vectors. For this work, the lattice vectors are assumed to remain orthogonal unit vectors that simply rotate at the lattice spin rate.

$$\dot{\mathbf{d}}_s = \Omega_l \cdot \mathbf{d}_s \tag{8}$$

$$\dot{\mathbf{n}}_s = \Omega_l \cdot \mathbf{n}_s \tag{9}$$

To complete the constitutive model, equations for the slip rates, $\dot{\gamma}_s$, are needed. For the model, a slip rate with a power-law dependence on the resolved shear stress as originally suggested by [7] was used.

$$\frac{\dot{\gamma}_s}{\dot{\gamma}_0} = \frac{\tau_s}{\kappa_s}\left|\frac{\tau_s}{\kappa_s}\right|^{(1/m-1)} \tag{10}$$

where $\dot{\gamma}_0$ is the reference slip rate, m is the rate sensitivity factor, τ_s is the resolved shear stress on slip system *s*, and κ_s is an internal state variable which accounts for the hardening on slip system *s*. The initial value of κ_s on each slip system corresponds to the critical resolved shear stress on that system, i.e. the stress necessary on slip system *s* to activate slip in the rate insensitive limit. One can extract the yield surface in stress space for a crystal from the κ_s values. The resolved shear stress, τ_s, for slip system *s* generated by an applied Cauchy stress, σ, can be obtained using Schmid's equation:

$$\tau_s = \mathbf{P}_s : \sigma \tag{11}$$

Evolution of hardening

The internal state variable κ_s in equation (7) represents the resolved shear strength of slip system *s*. In a polycrystal plasticity formulation such as the one outlined in the previous sub-section, work hardening is governed by the evolution of κ_s during deformation. The following relationship is employed for an anisotropic work hardening model: [2]

$$\kappa_s = \sum_{t=1}^{12} \mathrm{H}_{st} d\gamma_t \tag{12}$$

where H_{st} is a value taken from a matrix **H** of hardening moduli relating the hardening rate on slip system *s* to strain rate on slip system *t*. Obviously, in FCC metals **H** is a 12 x 12 matrix. The matrix **H** is always defined such that an active slip system hardens itself differently than it hardens other systems. Thus, the diagonal terms in **H**, where s=t, describe the self-hardening moduli for each slip system while the off-diagonal terms in **H** describe the latent-hardening moduli for each slip system. Attempts to model the hardening behavior of single crystals subjected to plastic deformation via equation (12) invariably propose that **H** evolves during deformation. Two separate anisotropic work hardening models developed to simulate the deformation response of FCC single crystals have been implemented into JAS-3D. One model was originally defined by Asaro [1] [4] [8], then later modified by Zhou et al. [9] and the other model was derived by Bassani and Wu. [10] [11] A part of this report considers the benefits and drawbacks of applying each anisotropic model as well as an isotropic hardening model, where all slip systems harden equally, to polycrystalline simulations.

Anisotropic evolution of hardening: modified Zhou model

The self hardening modulus in the modified Zhou model is defined as:

$$H_{ss} = h_0 \left(\frac{h_0 \gamma_s}{n \tau_0} + 1 \right)^{n-1} \tag{13}$$

where, h_0 and n are constants, respectively defined as the hardening modulus and work hardening exponent. τ_0 is also a constant, defined as the initial critical resolved shear stress of each slip system, set to the same value on each slip system. The modified Zhou model employs equation (14) to define the cross hardening terms of the hardening matrix **H:**

$$\boxed{H_{st} = q_{st} H_{ss}} \tag{14}$$

where, each coefficient in the matrix **q** is defined as a latent hardening ratio between slip system *s* and slip system *t*. In FCC crystals q_{st} is always greater that 1, indicating that if slip occurs on system *s*, the concomitant increase in hardening modulus on slip system *t* is always equal to or greater than the increase in hardening modulus on slip system *s*. The net result is that slip system *t*, the latent system, hardens faster than slip system *s* the active system. Following the slip system definition in Table I, the **q** matrix takes the form of equation (15):

$$\mathbf{q} = \begin{pmatrix} 1 & q_c & q_c & q_v & q_l & q_l & q_c & q_l & q_l & q_v & q_l & q_l \\ q_c & 1 & q_c & q_l & q_c & q_l & q_l & q_v & q_l & q_l & q_v & q_l \\ q_c & q_c & 1 & q_l & q_l & q_v & q_l & q_l & q_v & q_l & q_l & q_c \\ q_v & q_l & q_l & 1 & q_c & q_c & q_v & q_l & q_l & q_c & q_l & q_l \\ q_l & q_c & q_l & q_c & 1 & q_c & q_l & q_v & q_l & q_l & q_v & q_l \\ q_l & q_l & q_v & q_c & q_c & 1 & q_l & q_l & q_c & q_l & q_l & q_v \\ q_c & q_l & q_l & q_v & q_l & q_l & 1 & q_c & q_c & q_v & q_l & q_l \\ q_l & q_v & q_l & q_l & q_v & q_l & q_c & 1 & q_c & q_l & q_c & q_l \\ q_l & q_l & q_v & q_l & q_l & q_c & q_c & q_c & 1 & q_l & q_l & q_v \\ q_v & q_l & q_l & q_c & q_l & q_l & q_v & q_l & q_l & 1 & q_c & q_c \\ q_l & q_v & q_l & q_l & q_v & q_l & q_l & q_c & q_l & q_c & 1 & q_c \\ q_l & q_l & q_c & q_l & q_l & q_v & q_l & q_l & q_v & q_c & q_c & 1 \end{pmatrix} \tag{15}$$

The coefficients q_c, q_v, and q_l are latent hardening ratios based on experimental measurements on single crystals and the types of junctions formed between dislocations active on different slip systems. This report only considers the anisotropic hardening response of annealed FCC copper, and in this version of the model the coefficients q_c, q_v, and q_l are constant and set equal to 1, 1.5 and 1.7 respectively.

Anisotropic evolution of hardening: Bassani and Wu model

Beginning with the anisotropic work hardening basis given in equation (12). The form of the self hardening term is:

$$H_{ss} = f(\gamma_s)g(\gamma_t) \tag{16}$$

where $f(\gamma_s)$ represents the self-hardening of slip system *s* and $g(\gamma_t)$ represents the cross hardening of slip system *s* as a result of the total plastic strain accumulated on slip system *t*. In the JAS-3D implementation of the Bassani and Wu model, an inactive slip system does not harden, thus truly latent hardening is ignored, resulting in setting q=0 in a cross-hardening equation such as equation (14). This assumption follows that made by Bassani and Wu [10][11] in their original derivation of the model.

The functions $f(\gamma_s)$ and $g(\gamma_t)$ in equation (16) assume forms which fit the single crystal tensile deformation response of FCC metals. They are:

$$f(\gamma_s) = (h_0 - h_s)\sec h^2\left(\frac{(h_0 - h_s)}{\tau_1 - \tau_0}\right) + h_s \tag{17}$$

$$g(\gamma_t) = 1 + \sum_{t=1}^{12} f_{st} \tanh\left(\frac{\gamma_t}{\gamma_0}\right) \tag{18}$$

where, τ_0 is the initial critical resolved shear stress in each slip system, same as previously defined in equation (13). h_0, h_s, $\tau_1$and γ_0 are constants whose values can be extracted from the single crystal stress-strain response of the FCC material of interest. In the JAS-3D implementation the values of those constants are: $h_0=90\tau_0$, $h_s=1.5\tau_0$, $\tau_1=1.3\tau_0$ and $\gamma_0=10^{-3}$. f_{st} is a 12 x12 matrix of cofactors that relates the strength of the dislocation intersections between slip systems *s* and *t*, analogous to the **q** matrix defined for the modified Zhou model.

$$\mathbf{f} = 8 * \begin{pmatrix} 0 & f_c & f_c & f_v & f_l & f_s & f_c & f_l & f_l & f_v & f_s & f_l \\ f_c & 0 & f_c & f_l & f_c & f_l & f_l & f_v & f_s & f_s & f_v & f_l \\ f_c & f_c & 0 & f_s & f_l & f_v & f_l & f_s & f_v & f_l & f_l & f_c \\ f_v & f_l & f_s & 0 & f_c & f_c & f_v & f_s & f_l & f_c & f_l & f_l \\ f_l & f_c & f_l & f_c & 0 & f_c & f_s & f_v & f_l & f_l & f_v & f_s \\ f_s & f_l & f_v & f_c & f_c & 0 & f_l & f_l & f_c & f_l & f_s & f_v \\ f_c & f_l & f_l & f_v & f_s & f_l & 0 & f_c & f_c & f_v & f_l & f_s \\ f_l & f_v & f_s & f_s & f_v & f_l & f_c & 0 & f_c & f_l & f_c & f_l \\ f_l & f_s & f_v & f_l & f_l & f_c & f_c & f_c & 0 & f_s & f_l & f_v \\ f_v & f_s & f_l & f_c & f_l & f_l & f_v & f_l & f_s & 0 & f_c & f_c \\ f_s & f_v & f_l & f_l & f_v & f_s & f_l & f_c & f_l & f_c & 0 & f_c \\ f_l & f_l & f_c & f_l & f_s & f_v & f_s & f_l & f_v & f_c & f_c & 0 \end{pmatrix} \tag{19}$$

Model results

Finite element implementation

The JAS-3D finite element implementation of the microstructure mechanics model provides a framework to simulate the elastic-plastic deformation of an assemblage of grains representing a polycrystal. Typical simulations consist of 10,000-50,000 finite elements and 50-200 grains. Figure 1 illustrates results of a typical simulation, it shows the distribution of Von-Mises stress in a 3-D 30x30x30 model composed of 54 randomly oriented grains subjected to a prescribed displacement designed to simulate a tension test. Periodic boundary conditions were applied to all "surfaces" of the cube. The periodic boundary conditions used in the JAS-3D polycrystal plasticity simulations are a generalization of classical periodic boundary conditions. In classical periodic boundary conditions, the displacement of a node on one face is identical to the displacement of the corresponding node on the opposite face. In this case, that concept is generalized to allow an overall average displacement of an entire face to be imposed on the periodic displacement. This average displacement may be kinematic, i.e. user imposed displacement, or may be defined iteratively such as the average displacement to achieve an imposed overall force.

The overall stress-strain response of the polycrystal illustrated in figure 1 approximates the experimental tensile response of polycrystalline Copper. However, the geometric constraints imposed by neighboring grains within the polycrystal create large local variations in stress. These variations of stress and strain provide initiation sites for fracture, account for the variable and statistically dependent deformation response of polycrystalline materials and can contribute to localized strain-enhanced coarsening of microstructure, leading to thermomechanical fatigue and failure of a polycrystalline material. More importantly, a standard continuum model cannot predict the stress and strain variations observed in figure 1.

The microstructure mechanics, or polycrystal plasticity model, used to generate the results in figure 1 employed the Bassani [11] anisotropic work hardening model for Copper. Data and parameters for the same work hardening model have also been developed for Aluminum. Figure 2 illustrates the tensile response of a simulated two-phase material where the softer matrix phase is simulated using the parameters for Aluminum and the harder particulate phase is simulated using the properties for Copper. The composition of the two-phase polycrystal is 82.5%Al-17.5%Cu. The response of the two-phase polycrystal is compared with that of a two-phase material where each phase is treated as a continuum. Figure 2(a) shows that the simulated stress-strain response of the two-phase polycrystal and two-phase continuum is nearly identical to 5% strain. However, figure 2(b) and 2(c) reveal dramatic differences in the stress distributions of the two models. The difference in local stress distribution results from the inherent geometric effects between grains in the microstructural mechanics-polycrystal plasticity model which are not accounted for in a standard continuum-based model.

Grain rotations and the evolution of texture

Texture, or grain orientation distributions, and the evolution of texture can be measured experimentally, while local stress and strain distributions can not. Thus, tracking the evolution of texture during deformation provides perhaps the only method of validation for this type of microstructure-based simulations. At the one element per grain scale, isochoric deformation simulations were performed using the polycrystal plasticity model to validate and assess the models' predictive capability by tracking the evolution of texture during deformation. Figure 3 compares the evolution of fiber texture as predicted by the model when solved using an upper-bound solution, shown in figure 3(a), and using JAS-3D where each finite element represents a single grain in the polycrystal, shown in figure 3(b). Experimental data [12] has been superimposed on the upper-bound solution. The illustrated results demonstrate that the model predicts the evolution of fiber texture correctly. The meandering grain rotation paths shown in figure 3(b) for the finite element solution result from the local and changing variations in constraint during deformation of the polycrystal. Also, the meandering grain rotation paths slow the evolution of texture in the JAS-3D solution, providing a more comparable solution relative to the experimental results.

By extending the model to several hundred elements per grain, predictions of subgrain rotation and formation can be provided by the model and directly compared with Orientation Imaging Microscopy (OIM) collected using a specially equipped SEM which provides local crystal orientation data. Figure 4(a), a ⟨100⟩ pole figure, and 4(b) illustrate OIM data collected on the surface of an annealed copper tension specimen. The data was collected at a 2 μm spacing, then modified for model input as illustrated in figure 4(c). The modification procedure averages orientation measurements within each grain, which contain a small amount of scatter, to a single orientation. Figure 4(a) shows the effect of the modification procedure on the ⟨100⟩ pole figure where the red patches representing OIM measurements are reduced to single black points, each point representing an averaged grain orientation. Figure 4(d) shows the simulated distribution of misorientations relative to original grain orientation for the section of polycrystal on

the surface of the tension specimen deformed to 10% strain in the horizontal direction. The OIM technique provides grain orientation information only on the surface of the specimen and in this simulation the grains were extended 10 μm deep then constrained by a symmetry boundary condition. A comparison between simulated and experimental data of subgrain formation and rotation within a single grain is shown in figure 4(e) using an inverse pole figure representation. At 5% and 10% strain, the simulated data, shown in green and red, does not generally agree with the experimental data, shown in blue and yellow, in this figure. Approximated boundary conditions or lack of a length scale are possible reasons for the marginal simulation vs. experimental agreement of subgrain rotations at this size scale.

Work hardening model comparison

Anisotropic hardening models similar to the Asaro model discussed in the previous section has been the preferred hardening model in most crystal plasticity type simulations. In these models, the hardness, or resistance to deformation, of an individual slip system is defined in terms of the slip accumulated along other slip systems, as specified by equation (12). Such cross hardening rules are quite general but cumbersome to implement and slow finite element simulation solutions. Also, to address problems of interest to Sandia, a hardening model framework that incorporates a back-stress for fatigue simulations was necessary. Incorporating a back-stress into an Asaro-type anisotropic hardening model is difficult if not impossible, whereas incorporating a back-stress into an isotropic hardening model is straightforward and tractable. The isotropic hardening formulation for the polycrystal plasticity model implemented into JAS-3D has the following form:

$$\tau = \tau_0 + A\varepsilon^n \tag{20}$$

where A, n and τ_0 are constants, ε is equivalent plastic strain and τ is the strength of each slip system.

Figure 5 shows finite element polycrystal plasticity simulation results on a 40x40x40 polycrystal with 200 grains using both isotropic, shown in figure 5(b), and anisotropic, shown in figure 5(c), hardening models. A prescribed displacement with generalized periodic boundary conditions designed to simulate a tension test was applied to the polycrystal and periodic boundary conditions were applied to all "surfaces" of the cube, similar to analysis presented in figure 1. Figure 5(a) compares the engineering stress and strain response for both the isotropic and the anisotropic hardening models, and experimental data. Both models used parameters to give a good fit to the experimental stress-strain data. Only very minor quantitative differences are observed in the simulated stress distributions within the polycrystals. Thus the simple isotropic hardening model suffices and may prove superior for the polycrystal plasticity simulations of interest to Sandia.

To further understand the effect of slip system level work hardening formulations, the evolution of a 200 grain random textured polycrystal yield surface was predicted using JAS-3D polycrystal plasticity model with both anisotropic and isotropic work

hardening formulations. The polycrystal was produced from a two-dimensional Potts model simulation. This geometry was translated onto a one-element thick finite element mesh. The Potts model was not produced with a periodic grain structure so nominal boundary conditions were imposed to load the polycrystal structure along various load paths in plane-stress. The initial yield surfaces produced by these analyses, representing an annealed polycrystal, are shown in the figure 6(a), the data fits well to superimposed isotropic yield surfaces. The polycrystal was then loaded to approximately 50% prestrain in the $+\sigma 22$ direction, relaxed back to a stress-free condition and the yield surface was again probed. These results are shown in figure 6(b). At 50% prestrain there is a yield surface shift commonly associated with a back stress and an anisotropic evolution of the yield surface in both isotropic and anisotropic hardening models. The anisotropy and shift of the evolved data in figure 6(b) may be qualitatively gauged by comparing it to the superimposed isotropic yield surface. The anisotropic mechanical response generated by the isotropic hardening model simulation demonstrates the mechanical anisotropy in a polycrystalline material is governed at least in part by the geometric constraints and rotations of grain in the polycrystal and not slip system hardness anisotropy. Again, the isotropic hardening model results are nearly indistinguishable from the anisotropic hardening model results.

Mesh refinement study

The intent of the mesh refinement study was to determine if simulations using the JAS-3D polycrystal plasticity model exhibited a dependence on mesh or element size. To permit mesh refinement with elements other than quadrilaterals, the grain boundary triple points from a one element thick Potts model grain structure were extracted and straight edge grain boundaries were imposed between these points. By using a mesh paving algorithm, three finite element meshes were produced using the triple points and straight edge grain boundaries as guides. A generalized periodic boundary condition with an extension displacement was imposed on the top and bottom edges. The left and right edges, and front and back faces had a generalized periodic boundary condition which iteratively imposed a zero net force. Again, these boundary conditions were meant to simulate a tension test. The engineering-stress vs. engineering-strain results shown in figure 7(a) reveal indistinguishable macroscopic mechanical responses for finite element solutions using the three different meshes. Figure 7(b) illustrates that there is no mesh sensitivity in the stress distribution results. These simulations use the isotropic work hardening model, τ is the same for all slip systems and it is the variable that is plotted in figure 7(b). A characteristic length which may be defined in these simulations is the finite element size, e.g. more finite elements per grain is equivalent to a larger grain size. If the average finite element size is given a unit value, then the relative grain sizes are illustrated on the right-hand side of figure 7. The large change in relative grain sizes between the three simulations and the lack of grain size strengthening revealed in figure 7(a) provides an excellent demonstration of the effect of an undefined length scale endemic in these type of simulations.

Iteratively coupled simulations of polycrystal plasticity and microstructural evolution

In order to model the interdependence of microstructure and mechanical state, we coupled polycrystal plasticity simulations and microstructural evolution models. The polycrystal plasticity simulations were performed using Sandia's Jas3D FEM code, as described above. These plasticity simulations provide information about the local stress and strain states in a polycrystal, and Cu was chosen as a model system for this study. The local stress and strain data were supplied to grain growth simulations to ascertain the effects of deformation on boundary migration. The capability to integrate the two simulation approaches, i.e., plasticity and grain growth, was demonstrated.

The polycrystal plasticity simulation tracks numerous local mechanical variables such as stresses, strains, and lattice rotations. For the purposes of this study, we considered the effects of stress and plastic strain on grain boundary migration. To do this, we coupled two different grain growth models to the relevant outputs from the plasticity simulations. In the first case, the effects of plastic flow on grain growth in heavily deformed Cu were examined using a three-dimensional Monte Carlo Potts model (MCPM). In the second, a two-dimensional dynamic front tracking (FT) scheme was used to study the effects of elastic stresses on boundary migration in a slightly deformed material. These approaches and their results are summarized below.

Plasticity and the Monte Carlo Potts Model

The MCPM provides a lattice-based thermodynamic model of grain growth [13-15]. In this approach, a polycrystalline microstructure is digitized into voxels (or pixels in two dimensions) which are assigned integer identities. Collections of like voxels comprise a grain, and the interfaces between unlike voxels are grain boundaries, as depicted for a two-dimensional microstructure (with pixels) in figure 8. The evolution of this digitized microstructure is accomplished by using a Monte Carlo procedure to minimize a system Hamiltonian that assigns an energy to each unit of grain boundary. Specifically, the Potts Hamiltonian is

$$H = \frac{E_0}{2}\sum_{j=1}^{N}\sum_{i=1}^{z}\left[1-\delta\left(s_i,s_j\right)\right], \tag{21}$$

where E_0 is a positive constant which scales the boundary energy, N is the total number of lattice sites, z is the number of nearest neighbors j of site i, s_i is the voxel value or "spin" of lattice site i, and δ is the Kronecker delta function with $\delta(s_i,s_j) = 1$ if $s_i = s_j$ and 0 otherwise. When a Metropolis Monte Carlo (or equivalent) algorithm is used to minimize this function with respect to the lattice spins, s_i, the system's trajectory toward equilibrium correctly reproduces grain growth behavior in pure isotropic polycrystals.

The Hamiltonian in equation 21 describes the total energy of the grain boundaries in a polycrystal. When a material is stressed, the work of deformation is stored in the material as dislocations and/or elastic energy. The migration of grain boundaries in a

deformed material changes the stress state and redistributes stored dislocations, thereby altering the deformation energy stored within the grains. Thus, in order to treat grain growth in deformed polycrystals using the MCPM, the stored deformation energy must be included in the system Hamiltonian,

$$H = \sum_{i=1}^{N}\left\{\frac{E_o}{2}\sum_{j=1}^{z}\left[1-\delta\left(s_i,s_j\right)\right]+\frac{1}{V_i\tau_o}\sum_{\Delta l=0}^{\Delta l_f}\sum_{\alpha=1}^{12}\Delta\tau_i(\alpha,\Delta l)\Delta\gamma_i(\alpha,\Delta l)\right\}, \tag{22}$$

where V_i is the volume of lattice site i, τ_o is the initial (pre-hardened) critical resolved shear stress, $\Delta\tau_i$ and $\Delta\gamma_i$ are the shear stress and strain increments in site i on slip system a during deformation increment Δl, the sum over Δl includes all deformation increments up to the final deformation Δl_f, and the sum over a includes all 12 FCC slip systems. Thus, the first term in equation 22 represents the grain boundary energy and the second term is the stored plastic deformation energy. It should be noted that a more appropriate measure of stored plastic energy would be proportional to the dislocation density, which can be estimated [16] as

$$\rho \cong \left[\frac{\left(\tau_c-\tau_o\right)}{\beta G b}\right]^{\frac{1}{2}}, \tag{23}$$

where ρ is the dislocation density, τ_c is the strain-hardened critical resolved shear stress, β is a constant ranging from 0.3 to 0.6, G is the shear modulus, and b is the Burgers vector.

Performing a MCPM simulation using the system Hamiltonian in equation 22 minimizes the grain boundary energy and the stored plastic energy. In this study, we assume that a region of material (e.g., a voxel) that is "swept" by a moving grain boundary assumes the average plastic energy of all the neighboring voxels of the same spin value. (It might be more realistic to assign these swept voxels to zero stored plastic energy, meaning that all the dislocations are absorbed by the passing grain boundary. But without detailed knowledge of the interactions between the grain boundary and the stored dislocations, which are not treated by the plasticity simulation, the choice in this regard is somewhat arbitrary.) The "lattice" sites in the MCPM are taken to be the HEX elements of the plasticity simulation (described above), such that the grain growth and plasticity simulations share the same "mesh." (In practice, non-axisymmetric lattice sites, such as those in a deformed finite element mesh, produce unrealistic grain growth behavior. An alternative and correct approach would be to interpolate the plasticity data onto a cubic Potts lattice on which the grain growth simulations could be performed. However, this approach would complicate the transfer of data between the two simulations, since they would not share a common geometrical framework.) An example of such a simulation is provided in figure 9, which shows the evolution of the stored plastic energy (i.e., the second term in equation 22) during grain growth in a Cu polycrystal after 30% elongation. The stored plastic energy can counter the boundary energy's drive to maintain compact grain shapes, and thus grain boundary roughening occurs. This corresponds to

strain-induced boundary migration (SIBM) [17] observed in real polycrystals. As the grains grow, the material that is left behind contains relatively little stored plastic energy. (The blue grains that survive in the last frame of figure 9 are not the same grains that persist if the same microstructure is evolved without considering deformation.) A series of simulations like the one in figure 9 indicates that the rate of grain growth increases with increasing deformation, as shown in figure 10.

Plasticity and 2D Front Tracking

Whereas the MCPM takes a lattice-based thermodynamic approach to grain growth, the Front Tracking (FT) method utilizes continuum dynamics to simulate boundary migration. In the FT approach, each grain boundary is represented by a series of points that lie along the boundary, as depicted in figure 11. The motion of the boundary is dictated by the local boundary curvature at each point. This curvature can be calculated for a two-dimensional microstructure by fitting a circle between triplets of adjacent points and assigning the inverse of the circle's radius to be the local curvature. (More sophisticated methods, such as computing curvatures by fitting polynomial functions through the boundary points, can also be used but are generally more computationally expensive.) The curvature-based FT approach also correctly reproduces grain growth behavior in pure isotropic polycrystals.

The velocity of each boundary point in the FT scheme is

$$v = M\gamma\kappa, \tag{24}$$

where v is the velocity, M is the mobility of the boundary, κ is the local curvature of the boundary at the point of interest, and γ is the energy per unit area of the boundary and is analogous to E_0 in equation 21. In this study, the mobility and energy are assumed constant. The velocity vector lies perpendicular to the boundary and points toward the center of curvature. The term, $\gamma\kappa$, is simply the capillary pressure acting on the interface due to its curvature. When the polycrystal contains stored energy due to deformation, the additional pressure is simply the difference between the values of the stored energy per unit area (in two dimensions) on either side of the boundary. Thus, the velocity of a boundary point in a deformed polycrystal is

$$v = M_\kappa\gamma\kappa + M_\sigma\Delta U \tag{25}$$

where M_κ is the mobility of the boundary in response to the capillary pressure, M_σ is the mobility of the boundary in response to the elastic pressure, and ΔU is the difference in stored energy across the grain boundary. The pressure due to stored deformation energy acts perpendicular to the boundary and toward the region of lower stored energy. In this portion of the study, and unlike in the MCPM simulations described above, we treated only elastically deformed polycrystals. Thus, the stored energy, U, in the materials is

$$U = \sigma^T S \sigma \tag{26}$$

where σ is the six-component stress vector and S is the stiffness matrix. The stiffness matrix was computed using elastic constants for Cu, i.e., C_{11} = 168.4, C_{12} = 121.4, and C_{44} = 75.4, where all values are in GPa.

The FT method simulates boundary migration by evaluating the velocity of each boundary point according to equation 25, and then displacing each point by a distance $v\Delta t$, where Δt is a chosen time increment. At each step in a two-dimensional simulation, points that lie on grain boundary intersections (i.e., triple points) are positioned such that the angles of intersection of the three relevant boundaries are maintained at 120°. In this study, the stress state in the polycrystal was obtained from two-dimensional simulations of deformation, as described above, and the initial grain boundary points in the front tracking simulation correspond to nodes in the finite element mesh. This serves partly to facilitate the coupling between the FT and plasticity simulations. To simplify the treatment of stored elastic energy, the value of the stored energy in each grain is a constant and is taken as the average over all the finite elements in the grain. (The capability to iteratively couple the deformation and FT simulations, and thereby to consider the redistribution of stress due to grain growth, was established but not pursued due to time constraints. The treatment of local variations in the stored elastic energy was not explored due to time constraints.)

Figure 12 contains an example of a FT simulation of grain growth in a two-dimensional Cu polycrystal elongated by 1%. Since the stored energy is constant within each grain, and the FT simulations are deterministic (unlike the stochastic MCPM), grain boundary roughening due to SIBM is not observed. (Boundary roughening would occur only if local variations in the stored energy were considered.) However, the stored elastic energy can still counter the action of the boundary energy to maintain compact grain shapes, as evidenced by the elongated grains in the latter frames in figure 12. As the grains grow, the material that is left behind contains relatively little stored plastic energy, just as in the MCPM simulations. (As before, the blue grains that survive in the last frame of figure 12 are not the same grains that persist if the same microstructure is evolved without considering deformation.) A series of simulations like the one in figure 12 indicates that the rate of grain growth increases with increasing M_σ:M_κ ratio, suggesting that the rate of grain growth increases with increasing deformation, as shown in figure 13.

In order to demonstrate coupled simulations of polycrystal plasticity and microstructural evolution, the output from Jas3D plasticity simulations was used as input to a Monte Carlo Potts model (MCPM) and a front tracking (FT) model of grain growth. The MCPM simulations were used to examine the effects of stored plastic energy on grain growth, and the FT simulations treated stored elastic energy. In both cases, deformation produced non-compact grain shapes and promoted the growth of grains with relatively low stored deformation energy. The rate of grain coarsening was found to increase with increasing deformation. The capability to couple the simulations by performing multiple iterations of deformation and grain growth was established, but was not pursued extensively in order to focus on model development.

Brittle failure in Alumina stronglink materials

Dynamically coupled microcracking simulations

In this project, a microstructure-based computational cracking model, named GLAD (Grain Level Aging/Degradation) was developed and directly coupled with PARGRAIN, a dynamic Monte Carlo Potts model (MCPM), to explore effects of microstructure on crack initiation and propagation in material. In order to allow more accurate description of various material behaviors and obtain better numerical efficiency, the coupled PARGRAIN/GLAD was then extended and merged into a single code based on the Material Point Method (MPM). This meshless MPM code being developed is the first simulation code capable of modeling large heterogeneous deformation in structure, damage initiation and propagation in material, and coupled microstructural evolution and mechanical deformation. A wide range of material behaviors from long term aging to manufacturing can be studied via either quasi-static or dynamic simulations once the code is fully developed.

GLAD

GLAD is a discrete micromechanical model. It was developed to model deformation and brittle fracture in an elastic continuum. Rather than discretizing the equations of elasticity, the elastic continuum is discretized to a multi-dimensional array of lattice points connected by bonds [18-24]. These bonds act as torsional (resist bending), friable (breakable), zero mass (no rebound) springs. The energy of spring i is given by

$$E_i = \frac{1}{2}\sum_{j}^{nn}\Phi_{ij}(R_{ij}) + \frac{1}{6}\sum_{j}^{nn}\sum_{k}^{2}\Psi_{ijk}(\vec{R}_{ij},\vec{R}_{ik}) \tag{27}$$

where the outer sums are over the j nearest neighbors of i, the inner sums are over the k shared neighbors of sites i and j, and $\vec{R}_{ij}$ is the vector separation of sites i and j of magnitude R_{ij}. The function Φ represents the energy due to the linear elastic extension of an ideal spring:

$$\Phi_{ij} = \frac{1}{2}k_{ij}\left(R_{ij} - a_o\right)^2 \tag{28}$$

where k_{ij} is the spring constant and a_o is the unstressed spring length. Similarly, Ψ is the energy of bending an ideal torsional spring:

$$\Psi_{ijk} = \frac{1}{2}c_{ijk}\left(\frac{\vec{R}_{ij}\bullet\vec{R}_{ik}}{R_{ij}R_{ik}} - b_o\right)^2 \tag{29}$$

where c_{ijk} is the bending spring constant and b_o is the cosine of the unstressed angle between springs i, j, and k. At some critical spring energy E_i^c, spring i breaks and all its

spring constants are reset to zero. Both the spring constants, which are related to stiffness, and the breaking energy, which is related to surface formation energy, can differ for bulk and boundary springs. Microstructural features may be incorporated into the model by associating different properties with each spring. For example, a polycrystalline body may be simulated by identifying a bond as a bulk bond if it separates two adjacent lattice sites within the same grain and as a grain boundary bond if it separates two adjacent lattice sites belonging to different grains. Different material constants, e.g. Young's modulus, Poisson's ratio and coefficient of thermal expansion, etc, may be assigned at each bond to model anisotropy. Figure 14 gives a schematic example of a 2D triangular GLAD model. The microstructures in this study were equiaxed, single phase polycrystalline grain structures produced using the Monte Carlo Potts Model grain growth simulation.

A uniaxial stress is incrementally applied to the spring network, and a conjugate gradient method is used to minimize system energy by stretching and breaking springs. This process is repeated until the system is fractured into two parts. The system deforms as an inhomogeneous, elastic solid [18]. Stress concentrations do occur at crack tips, but at a lower than theoretical magnitude [19]. As is often the case in brittle polycrystalline metals and ceramics, fracture may occur in an intergranular, intragranular, or mixed mode. A simulated 2D result of fracture in mixed mode is shown in figure 15.

During the course of the research, a massively parallel version of 3D GLAD code was developed on various parallel computing platforms made by Intel, IBM, and SGI, etc. The code takes the 3D microstructures generated by PARGRAIN as input and performs mesoscale cracking simulations under user-specified deformations. GLAD is the first lattice mechanics code capable of modeling inter- and intragranular cracking in a 3D grain structure under quasi-static thermomechanical deformations. A result of anisotropic-thermal-expansion induced microcracking is shown in figure 16.

Coupled PARGRAIN/GLAD

One of the goals of this project was to determine the interplay between microstructural evolution and cracking under various conditions. In order to study this phenomenon, we dynamically coupled two codes that had been successful at modeling the two effects independently. The microstructural evolution code is PARGRAIN, which is a parallel Monte Carlo Potts model (MCPM) grain growth code with many speed optimizations built-in [25]. The cracking code is MPGLAD, which is the parallel GLAD code described above.

Coupling the two codes was conceptually straightforward given the nature of the two algorithms. They both were implemented on a square (or cubic, in the case of 3D) lattice, and the same lattice was used to handle the material representation in both codes. The cracking code was essentially unchanged with the exception that the material variables which represented the grains and grain boundaries became dynamic variables which change as a function of time. There were algorithmic changes that were necessary in the grain growth program related to the effects of cracking. In general, the MCPM model determines the probability of a site changing its orientation by considering the

orientations of all of its neighbors (8 for square lattice and 26 for the cubic lattice). The higher the number of neighbors of a similar orientation, the higher the probability of switching to that orientation. However, a crack separates a site from its neighbors, so it does not physically make sense for one to consider the "cut-off" site in the grain switching calculation. Thus, in the coupled simulation such sites were not included in the orientation change calculation.

There are two main ways in which the simulations affect each other. The first, as described previously, is that a growing crack can inhibit the growth of grains. This is especially true if a crack goes through an existing grain. In this case, the grain is usually doomed to be absorbed by neighboring grains. The other way in which the grain growth and cracking can affect each other is that as grains grow, the decrease in total grain boundary area can change the direction of the crack. If parameters are such that cracking is energetically more favorable along grain boundaries, then the cracks will be more likely to travel a longer distance to stay on the interface.

Because of these two effects, there were two parameters that were important to the shape of the resulting crack. The first was the ratio of the energy required to break an intergrain bond versus the energy to break an intragrain bond. The second parameter was the relative speed of the grain growth to that of the crack propagation. The most interesting scenario occurred when the intergrain cracks took about 70% of the energy to form as the intragrain cracks. Then one could see a clear effect of the cracks choosing to go around small grains (especially at the beginning of the simulation, when the most of the grains were small), but going through the larger grains. Snapshots from such a simulation are shown in figure 17.

Off-lattice MCPM

Another aspect of the project was that of testing different approaches to an off-lattice version of the MCPM. In this version, the "sites" of the previous lattice were replaced by polyhedral grains generated by various randomizing algorithms, including Voronoi tessellations of Poisson points and radical Voronoi tessellations of centers of systems of hard spheres. The only question then was that of how to determine the rules for orientation changes.

There are two fundamental differences between the off-lattice and lattice MCPM. The first is that the amount of surface area that two neighbors share is not constant in the off-lattice model. One would assume that for grain growth driven by boundary surface area, the amount of surface area between the two sites would be important. The second difference was that the volumes of the sites could all be different, meaning that an algorithm that chose to pick a site randomly to flip (or that simply chose the sites sequentially) would not necessarily make physical sense.

The problem of the different surface areas was handled by weighting the contribution of each neighboring site by its contribution to the total surface area of each site. This seemed to make the most sense physically. The question about how to weight each site when choosing which reorientation to attempt was not adequately resolved

before the project ended. However, there were many test runs of the program with different choices for the site weighting algorithm. Most of the simulations gave results similar to that of the on-lattice simulation, with the difference being that there were no effects related to lattice (such as pinning). Also, the resulting grains seemed to be visually more representative of actual physical samples than the lattice simulations. This work will continue under the ASCI/PZT program and the MICS program.

MPM

The goal of this part of effort is to develop a single code, based on the Material Point Method (MPM), with appropriate microstructural evolution and material mechanics models implemented. This MPM code, once fully developed, will be numerically efficient and capable of simulating phenomena of coupled microstructural evolution and mechanical deformation as well as material damage development at mesoscale. MPM uses both a Lagrangian and an Eulerian representation of solid bodies for studying their mechanical deformation. The Lagrangian representation is a set of material points chosen within each solid body that is tracked throughout the deformation history of the material being modeled. The Eulerian representation is a background computational grid that covers the computational domain, and where interactions between material points are calculated. The full numerical solution is calculated at the material points; for example, these points have mass, displacement, velocity, strain, stress, plastic strain, internal energy and temperature associated with them. To compute the interaction, the information carried by the material points is projected onto a background finite element mesh where equations of motion are solved in an updated Lagrangian frame. Information from this solution is then used to update the material points. Once the material points have been updated, the mesh can be discarded and a new one constructed to satisfy properties under the user's control. In the current work, a cubic mesh of elements in Cartesian geometry is used.

MPM uses continuum-based constitutive equations to describe various material behaviors. Therefore, complicated material response, such as anisotropic elasticity and plasticity, viscoelasticity and viscoplasticity, can be modeled appropriately. An interface was developed so the microstructures generated by PARGRAIN can be used by the MPM code as input for mesoscopic polycrystalline mechanics simulations. In addition, with a newly developed decohesion model implemented, MPM is capable of modeling crack/damage initiation and evolution in a microstructure. An example of 2D MPM simulation of anisotropic-thermal-expansion induced microcracking is given in figure 18. Figure 18(a) shows the initial MPM model based on a polycrystalline structure generated by PARGRAIN. Grain boundary was represented by a specially treated area with a finite thickness that was arbitrarily taken to be approximately two layers of material points. The decohesion model was assigned along all the grain boundaries. The arrows in figure 18(b) indicate the preferred thermal expansion direction chosen randomly for each grain. Microcracks started to develop when the temperature of the material dropped. The calculated damage level is shown by color shading in figure 18(b).

A novel research initiated in the current LDRD is to develop an MPM based algorithm for microstructural evolution simulations using discrete material particles. The

algorithm design is being based on a diffuse interface model (or phase field model) which gives a continuum description compatible with the MPM framework. The diffuse interface model is based on solution of the Cahn-Hilliard equation. [26] To employ the particle method, initial values of the composition and mass are assigned to each particle on the particle mesh. As the time step begins, the first step in the algorithm is to map these particle quantities to the grid using quadratic B-Spline interpolation. Next, the Cahn-Hilliard equation for the change in composition is solved on the grid using explicit forward differences in time and second-order centered differences in space. Finally, the grid values are interpolated to the particle mesh in order to update the composition values on the particles. The next time step begins by interpolating the updated particle quantities to the mesh and then the steps mentioned above repeat. Several test problems of coarsening in binary alloy have been analyzed in two dimensions to check the capability of the model. Results in figures 19 and 20 show two possible interactions of a small and large inclusion in the matrix phase. In figure 19, the initial separation between the inclusions is large enough so that the coarsening takes place through diffusion. In figure 20, there is coalescence since the two inclusions are initially quite close together. In the future, the current microstructural evolution will be expanded to include the effects of mechanical deformation when the funding is available.

Experimentally-based micromechanical simulations

Residual stresses arise in ceramics during processing as a result of thermal expansion anisotropy and crystallographic misorientation across the grain boundaries. During microstructural evolution, boundaries with higher mobilities and energies are eliminated, thereby changing the distribution of lattice orientations and misorientations. This process is expected to change the distribution of grain orientations (and misorientations) with increasing grain size to one that is less random. The magnitude and distribution of stresses therefore is likely to depend on the grain size and degree of texture in the samples.

Depending on the grain size, the residual stresses can cause spontaneous microcracking during the processing of these materials. In addition, the microstructural level stresses are likely to play a significant role in where cracks initiate and propagate under macroscopic loading.

Connecting experiment to simulation

The crystallographic orientations of grains in alumina (99.99% pure) and spinel ($MgAl_2O_4$) were determined using electron-backscattered diffraction (EBSD). EBSD patterns were collected and automatically indexed using TSL's Orientation Imaging Microscopy (OIM) software [27]. The relative grain boundary energies were determined by thermal groove geometries using atomic force microscopy (AFM) [28]. The ratio of grain boundary to surface energy was obtained using the simplified Herring equation: $\gamma_{gb}/\gamma_s=2\cos(\psi/2)$ where ψ is the surface dihedral angle. This equation assumes that the torque terms are zero, the surface energies are isotropic, and the grain boundary energy is a function of misorientation alone and not of the boundary plane inclination.

The magnitudes of residual stresses in alumina were predicted using object oriented finite (OOF) element analysis and experimentally determined orientations. OOF is an object oriented finite element analysis software program developed at NIST [29]. It is designed to investigate the response of real or simulated microstructures to mechanical and thermal loads. The program performs thermoelastic calculations in two dimensions (plane strain or plane stress) using 3-node triangular elements. The user specifies crystallographic orientations, elastic, and thermal properties for the various regions (grains) in the microstructure. Based on this information, a finite element grid with associated properties is generated on which mechanical and/or thermal loading can be applied. Crack initiation and propagation were also simulated in OOF using the Griffith fracture criterion. Grain boundary energies estimated by AFM groove measurements were used in the analyses.

A code (OIM2OOF) was developed that allows crystallographic orientations from Orientation Imaging Microscopy (OIM) to be directly imported into OOF. This code allows the user to analyze residual stress distributions in large microstructures (>600 grains) with relative ease. The code also detects grain boundaries and assigns respective relative grain boundary energies (obtained by groove measurements) automatically.

Microcracking during cooling in pure Alumina

Crystallographic orientations and relative grain boundary energies were determined in alumina and spinel samples using EBSD and AFM respectively. Two different grain size (10 and 27 μm) 99.99% pure alumina samples that were made by conventional sintering were analyzed. The texture and mesotexture (grain boundary misorientations) were random in both samples and no special boundaries were observed. There was no clustering of orientations and no apparent correlation between misorientation and γ_{gb}/γ_s [30]. The mean value of dihedral angle and γ_{gb}/γ_s for the 27 μm alumina was 110° and 1.14 and the corresponding values for spinel were 113° and 1.10 respectively.

Residual stresses in alumina (>650 grains) due to its thermal expansion anisotropy were estimated using OIM2OOF and OOF codes. The simulation used 73728 elements. The elastic stiffness constants and coefficients of thermal expansion for α-alumina (hexagonal crystal symmetry) used in the analysis were C_{11}=497 GPa, C_{12}=163 GPa, C_{13}=111 GPa, C_{33}=498 GPa, C_{44}=147 GPa, $\alpha_{11}=8.6\times10^{-6}$ /°C, and $\alpha_{33}=9.3\times10^{-6}$ /°C [31]. The calculations were done assuming plane stress and free boundary conditions. Figure 21 shows the microstructure (OIM output), stress invariant 1 ($\sigma_{11}+\sigma_{22}$), and maximum principal stress distributions for a temperature change of -1500°C. Very high stresses develop at the grain boundaries due to crystallographic misorientations in conjunction with the thermal expansion anisotropy in alumina. The highest value of the maximum principal stress was fairly high (≈480 MPa). The average stress in grains compares favorably with those measured by spectroscopic [32] and fluorescence imaging [33]. The highest stresses were localized at the grain boundaries and triple junctions and drop rapidly away from the boundaries. The maximum stress is comparable to typical fracture strength of this material. The residual stress distributions were almost identical in the 10

and 27 μm samples indicating no or negligible effect of grain size (orientations were random in both cases). It should be noted that the stress calculations are purely elastic and assume no stress relaxation mechanisms are active. In reality, diffusional flow, plastic deformation, and microcracking will relax the constraints between the grains and reduce the residual stresses. There appear to be regions of tensile and compressive stress on a scale that is larger than the grain size (figure 21c). Analysis is continuing to understand this observation.

In ceramics, cooling from the sintering temperature (≈1550°C for alumina) often creates sufficiently high stresses to cause microcracking. A part of the microstructure in figure 21 was analyzed for crack initiation and propagation using OOF. Details of the cracking simulation are presented elsewhere [34]. The ratios of grain boundary to surface free energies obtained using contact AFM imaging were used. The surface energy of grains was assumed to be isotropic and taken as 2 J/m^2. The grain boundaries were assigned elastic and thermal properties of glass (isotropic crystal symmetry), E=70 GPa, ν=0.23, and α=9.5x10^{-6}/°C. Figure 22 shows initiation and propagation of microcracks as the material is cooled from the sintering temperature. Cracks initiated at the triple junctions and propagated along the grain boundaries. With increasing temperature difference (thermal strain), microcracks initiated at new sites and coalescence of microcracks formed larger cracks. As can be seen, damage occurred at several regions and some of the boundaries were completely cracked.

The effect of grain size on the critical temperature for microcracking in alumina was determined using the microstructure in figure 22 by varying the dimensions of the image, i.e., different length scales were used to represent different grain sizes. The expected inverse square root grain size relationship was found, as shown in figure 23. The critical grain size for microcracking for an alumina sample cooled from a 1600°C sintering temperature with high CaO glass (α≈9.5x10^{-6}/°C) grain boundary phase was 179 μm and with high MgO phase (α≈5x10^{-6}/°C) was 71 μm. High CaO and high MgO compositions were chosen as they represent the bounds on the type of grain boundary glass phase typically found in alumina. Experimentally, critical grain size values have been reported between 40-100 μm [35]. It should be noted that plane stress conditions underestimate the residual stress values, hence in reality, the critical grain size values are expected to be lower.

Residual stresses were also predicted for textured alumina. The sample was textured in c-axis with MRD (multiples of random distribution) value of 90. As one would expect, the stresses were much smaller in this sample compared to "randomly-oriented" samples. The largest maximum principal stress was ≈ 425 MPa. Figure 24, shows the number of elements versus their stress value (stress invariant 1). The number of elements with high stresses is much lower in the textured sample than in the randomly-oriented sample. In both cases, the number of elements with high stresses is very small. In the "randomly-oriented" sample, <5% of the total elements had high stresses (>250 and <-250 MPa). The corresponding number in the textured sample was <0.4%.

Summary and Conclusions

Computational materials simulations have traditionally focused on an individual phenomenon: grain growth, crack propagation, plastic flow, etc. However, real materials behavior results from a complex interplay between phenomena. In this project, we explored methods for coupling mesoscale simulations of microstructural evolution and micromechanical response. In one case, massively parallel (MP) simulations for grain evolution and microcracking in brittle materials were dynamically coupled. In the other, codes for domain coarsening and plastic deformation were iteratively linked. The computer simulations were applied to stockpile materials. Microcracking in brittle materials was studied in the context of alumina used in stronglinks. Plastic deformation response was studied in a Ag-Cu eutectic braze alloy, used in weapon components.

This three-year project delivered a variety of capabilities, benefits, and advances to Sandia, including:

1. A suite of new computational capabilities

1. MP PARGRAIN (massively parallel Monte Carlo grain growth code, which produced the largest simulations of grain growth ever)

2. MP GLAD (massively parallel ball-and-spring model for fracture, the first ever in 3D)

3. OOF (Object Oriented Finite Element model for elasticity and fracture on the microstructural scale, incorporating full experimental data)

4. MPM (Materials Point Method for large strain deformations and for concurrent microstructural evolution, the first of its kind)

5. Polycrystal Plasticity (Finite Element code for micromechanics, the first with full periodic boundary conditions)

6. Front Tracking (continuum model for grain growth, the first implementation for strain-enhanced growth)

These applications combine new physical models and new computational algorithms to generate the most realistic simulations of microstructure and micromechanics ever performed.

2. The first fully coupled microstructure/micromechanics simulations

A spring model for fracture (MP GLAD) was coupled directly with a Potts model for grain growth (MP PARGRAIN) to model cracking during annealing of brittle ceramics. Computational successes in this work included timestep matching and scalable parallelization via spatial decomposition; the results elucidated the phenomenology of fracture.

A finite element model for microplasticity (Polycrystal Plasticity) was indirectly coupled with a Front Tracking model for grain growth to simulate strain-enhanced microstructural evolution. Computational successes included mesh matching and optimization of data handoff; the results reproduced strain-enhanced boundary migration (SIBM).

3. The first direct links between mesoscale simulations and OIM data

OIM microstructures were input into Object Oriented Finite Element (OOF) simulations to predict the elastic and fracture response of alumina ceramics upon cooling. Microcracks were found to originate at grain triple junctions. The critical grain size for microcracking was successfully predicted as a function of the glassy grain boundary phase and the crystallographic texture.

OIM microstructures of pure copper before and after deformation were compared to Polycrystal Plasticity simulations. The simulations reproduced macrotexture well; however the simulations did not accurately capture microtexture evolution. This is likely because the simulations do not include a substructure formation length scale necessary to model the subgrain formation that characterizes deformed copper.

4. An element-free Materials Point Method (MPM) for large-strain deformations coupled to microstructural evolution

The first massively parallel, three-dimensional MPM with periodic boundary conditions was implemented and tested. A boundary decohesion model was included in MPM to model microcracking, and a Phase Field model for coarsening was coupled with MPM to model microstructural evolution.

5. Extensive experimental testing and characterization of CuSil alloys and stronglink aluminas

6. Recognition of the problem of substructure length scale in current finite element implementations

An international workshop was held to address this problem, and based on the findings of the workshop, a proposal for solving this problem was funded to begin in FY00.

References

[1] Asaro, R.J. and Rice, J.R. "Strain Localization in Ductile Single Crystals", J. Mech. Phys. Solids, **25** 309-338 (1977).

[2] Hill, R. and Rice, J.R. "Constitutive Analysis of elastic-plastic crystals at arbitrary strain", J. Mech. Phys. Solids, **20** 401-413 (1972).

[3] Canova, G.R., Fressengeas, C., Molinari, A., and Kocks, U.F., "Effect of Rate Sensitivity on Slip System Activity and Lattice Rotation", Acta metall., **36** 1961-1970 (1988).

[4] Pierce, D., Asaro, R.J. and Needleman, A., "An Analysis of Nonuniform and Localized Deformation in Ductile Single Crystals" Acta Metall., **30** 1087-1119 (1982).

[5] Mika, D.P. and Dawson R. "Polycrystal Plasticity Modeling of Intracrystalline Boundary Textures" Acta Mater., **47** 1355-1369 (1999).

[6] U.F. Kocks, C.N. Tome and H.R. Wenk Texture and Anisotropy: Preferred Orientations in Polycrystals and their Effect on Material Properties, Cambridge University Press, Cambridge, England (1998).

[7] Hutchinson, J.W., "Bounds and Self-Consistent Estimates for Creep of Polycrystalline Materials", Proc. R. Soc. Lond. A, **348** 101-127 (1976).

[8] Asaro, R.J. and Needleman, A., "Texture Development and Strain Hardening in Rate Dependent Polycrystals" Acta metall., **33** 923-953 (1983).

[9] Zhou, Y., Neale, K.W. and Toth, L.S., "A Modified Model for Simulating Latent Hardening During the Plastic Deformation of Rate-Dependent FCC Polycrystals" Int. J. Plasticity, **9** 961-978 (1993).

[10] Wu, T.Y., Bassani, J.L., and Laird, C., "Latent Hardening in Single Crystals I. Theory and Experiments", Proc. R. Soc. Lond. A, **435** 1-20 (1991).

[11] Bassani, J.L. and Wu, T.Y. "Latent Hardening in Single Crystals I. Theory and Experiments", Proc. R. Soc. Lond. A, **435** 21-41 (1991).

[12] Stout, M.G. and O'Rourke, J.A. "Experimental Deformation Textures of OFE Copper and 70:30 Brass from Wire Drawing, Compression, and Torsion", Metall. Trans. A, **20** 125-131 (1988).

[13] M. P. Anderson, D. J. Srolovitz, G. S. Grest, and P. S. Sahni, "Computer Simulation of Grain Growth - I. Kinetics," Acta Metall. **32**[5] 783-791 (1984).

[14] D. J. Srolovitz, M. P. Anderson S. Sahni, and G. S. Grest, "Computer Simulation of Grain Growth - II. Grain Size Distribution, Topology, and Local Dynamics," Acta Metall. **32**[5] 793-802 (1984).

[15] M. P. Anderson, G. S. Grest, and D. J. Srolovitz, "Computer Simulation of Normal Grain Growth in Three Dimensions," Phil. Mag. B **59**[3] 293-329 (1989).

[16] G.E. Dieter, Mechanical Metallurgy (McGraw-Hill 1976) p. 147.

[17] P.A. Beck, in Metal Interfaces, edited by R.M. Brick (ASM, Cleveland, OH, 1952), pp. 208-47.

[18] P. D. Beale and D. J. Srolovitz, "Elastic Fracture in Random Materials", Physical Review B **37** 5500-5507 (1988).

[19] W. H. Yang, D. J. Srolovitz, G. N. Hassold and M. P. Anderson, "Microstructural Effects in the Fracture of Brittle Materials", in Simulation and Theory of Evolving Microstructures, eds. M. P. Anderson and A. D. Rollett (The Metallurgical Society, Warrendale, Pennsylvania, 1990), pg. 277-284.

[20] N. Sridhar, W. Yang, D. J. Srolovitz and E. R. Fuller, "Microstructural Mechanics Model of Anisotropic-Thermal-Expansion -Induced Microcracking", J. Am. Ceram. Soc. **77**[5] 1123-38 (1994).

[21] R. LeSar and D. J. Srolovitz, "Modelling of Transformation Toughening in Brittle Materials," Materials Science and Engineering A **155** 267-274 (1992).

[22] W. A. Curtin and H. Scher, "Brittle Fracture of Disordered Materials," J. Mat. Res. **5** 535-553 (1990).

[23] S. P. Chen, "Modeling of Brittle/Brittle Laminates: The Effects of the Interfacial Cohesion" Scripta Met. et Mat. **31** 1437-1442 (1994).

[24] W. A. Curtin, "Toughening in Disordered Brittle Materials," Phys. Rev. B **55** 11270-11276 (1997).

[25] S. A. Wright, S. J. Plimpton, T. P. Swiler, R. M. Fye, M. F. Young, E. A. Holm, "Potts-model Grain Growth Simulations: Parallel Algorithms and Applications," Sandia Report SAND97-1925, August 1997.

[26] Cahn, John W. and Hilliard, John E., "Free Energy of a Nonuniform System. I. Interfacial Free Energy", The Journal of Chemical Physics, **28**[2] 258-267 (1958).

[27] Orientation Imaging Microscopy (OIM) version 2.6, TexSEM Labs, Inc., Provo, UT (1998).

[28] D.M. Saylor and G.S. Rohrer, "Measuring the influence of grain-boundary misorientation on thermal groove geometry in ceramic polycrystals", J. Am. Ceram. Soc., **82** [6] 1529-36 (1999).

[29] OOF version 1.0.7, Center for Theoretical and Computational Materials Science (CTCMS), National Institute of Standards and Technology (NIST), Gaithersburg, MD (1999).

[30] S.J. Glass, V.R. Vedula, D.M. Saylor, and G.S. Rohrer, "Application of electron backscattered diffraction (EBSD) and atomic force microscopy (AFM) to determine texture, mesotexture, and grain boundary energies in ceramics", Proceedings of the Twelfth International Conference on Textures of Materials, Montreal, Canada, NRC Research Press, **2** 1489-94 (1999).

[31] J.B. Wachtman, W.E. Tefft, D.G. Lam, R.P. Stinchfield, "Elastic constants of synthetic single crystal corundum at room temperature", J. Res. Nat. Bur. Std., **64A** 213-28 (1960).

[32] Q. Ma and D.R. Clarke, "Piezospectroscopic determination of residual stresses in polycrystalline alumina", J. Am. Ceram. Soc., **77** [2] 298-302 (1994).

[33] R.H. Dauskardt and J.W. Ager, "Quantitative stress mapping in alumina composites by optical fluorescence imaging", Acta Mater., **44** [2] 625-41 (1996).

[34] V.R. Vedula, S.J. Glass, D.M. Saylor, G.S. Rohrer, and W.C. Carter, "Predicting microstructural level residual stresses and crack paths in ceramics", Proceedings of the Twelfth International Conference on Textures of Materials, Montreal, Canada, NRC Research Press, **2** 1507-12 (1999).

[35] E.D. Case, J.R. Smyth, and O. Hunter, "Microcracking in large grain Al_2O_3", Mater. Sc. Eng., **51** 175-9 (1981).

Appendix A: Experimental support

High temperature creep/fatigue testing of CuSil specimens

We proposed conducting high temperature creep / low-cycle fatigue tests on samples in the Ag/Cu system on the Gleeble 1500 thermomechanical simulator. This was mainly as a supplement to the work done on conventional test frames whose test chambers and dilatometers were limited to <600°F (316°C). In order to measure accurate dilatometry and mechanical test data using the Gleeble, several modifications needed to be made to the testing equipment. The existing 18,000 lb capacity load cell was impractical to do deformation studies on materials that are relatively soft such as copper, gold, or silver, especially at elevated temperatures, without requiring large diameter cross-sections (on the order of 1 inch) given that these are precious materials. Partly, this is because it would be operating at a low fraction of its capacity, but more seriously because it is located outside of sliding seals which maintain the integrity of the environmental chamber that the sample is in during testing. These seals exerted a variable frictional force that was found comparable to the force generated by the specimen. Thus, a low force load cell assembly which relocated the load cell inside the chamber, and which was capable of using a load cell with maximum capacity of 500 lbs was acquired and fitted to our present equipment. In learning how to use this retrofit we determined that while the loads that can be measured are now acceptable, due to the nature of the main electronic control loops, the Gleeble can not be safely operated in load control, but must be operated in stroke or strain control. While this limits what can be done experimentally, it is not really too serious, as fatigue and stress relaxation testing is normally done in these latter modes. It is a more serious impediment to creep testing, however, where a controlled load is desired.

Once the load measurement resolution problem was solved, several sample geometries including both tensile and compression types were evaluated (in consultation

with T. Buchheit Dept. 1835) that would allow the evaluation of small load tensile properties using stroke control for regions of plastic deformation. This basically involves the direct measurement of the reduction in cross-sectional area (with a high resolution diametral dilatometer) and measuring the true stress directly. These tests were performed using already available 304 Stainless steel specimens to prove the feasibility.

In addition, an alternative method of attaching thermocouples had to be validated for the Ag/Cu system creep / fatigue samples. Normal Gleeble practice involves welding a control thermocouple directly to the center of the specimen gauge length. This was deemed undesirable in creep/fatigue testing as it would introduce a discontinuity and would locally change the microstructure. (It is also difficult to weld the normal type K thermocouple reliably to Ag/Cu-base materials). An alternative method where a thermocouple was 'tied' onto the sample was developed. The Gleeble reference materials also suggested that some limitation of testing conditions would be encountered in such high electrical conductivity specimens (the Gleeble uses AC resistance heating to control specimen temperature). However, validation tests on pure Cu were successful and showed that the samples could still be heated at rates on the order of 10°C / s and held at temperatures of 400°C for extended periods of time. During these tests, the Gleeble did not appear to have any trouble controlling these cycles for pure copper specimens and thus there is no reason to believe it will not work for the CuSil specimens at temperatures up to the eutectic melting point.

Using the above steps, a sample geometry was identified and alternate methods of testing were chosen so that the eutectic CuSil specimens could be tested. Several specimens were machined and are ready for testing, but due to conflicts with other programs using the machine and operators and budget constraints, the actual fatigue testing of the specimens could not be completed in FY99.

Appendix B: Publications, Presentations, and Workshops

Journal Papers

Y.-L. Shen, W. Li, H. E. Fang, Phase Structure and Cyclic Deformation in Eutectic Tin-Lead Alloy: A Numerical Analysis, *Journal of Electronic Packaging* (submitted)

Y.-L. Shen, W. Li, D. L. Sulsky, H. L. Schreyer, Localization of Plastic Deformation Along Grain Boundaries in a Hardening Material, *International Journal of Mechanical Sciences* (submitted)

Veena Tikare, Elizabeth A. Holm, Simulation of Grain Growth and Pore Migration in a Thermal Gradient, *J. Amer. Ceram. Soc.*, v81[3], 1998, 480-484

Elizabeth A. Holm, The Surface Formation Energy for Intergranular Fracture in Two-Dimensional Polycrystal, *J. Amer. Ceram. Soc.*, v81[3], 1998, 455-459

E. A. Holm, N. Zacharopoulos, D. J. Srolovitz, Nonuniform and Directional Grain Growth Caused By Grain Boundary Mobility Variations, *Acta Materialia,* v46[3],1998, 953-964

M. Tabbara, A computational method for quasi-static fracture, *International Journal of Solids and Structures*, 1998.

Refereed Conference Proceedings

C. C. Battaile, E. A. Holm, T. Buchheit, G. Wellman, M. Neilsen, Coupled Simulations of Mechanical Deformation and Microstructural Evolution Using Polycrystal Plasticity and Monte Carlo Potts Models, *Mat. Res. Soc. Symp. Proc.*, v538, 1999, 269-273

S.J. Glass, V.R. Vedula, D.M. Saylor, G.S. Rohrer, Application of electron backscattered diffraction (EBSD) and atomic force microscopy (AFM) to determine texture, microtexture, and grain boundary energies in ceramics, *Proceedings of the Twelfth International Conference on Textures of Materials*, NRC Research Press, v2, 1999, 1489-1494

V.R. Vedula, S.J. Glass, D.M. Saylor, G.S. Rohrer, W.C. Carter, Predicting microstructural level residual stresses and crack paths in ceramics, *Proceedings of the Twelfth International Conference on Textures of Materials*, NRC Research Press, v2, 1999, 1507-1512

Corbett C. Battaile, Elizabeth A. Holm, Evolution of 2D Potts Model Grain Microstructures from an Initial Hillert Size Distribution, *Grain Growth in Polycrystalline Materials III*, H. Weiland, B. L. Adams, and A. D. Rollett (editors), TMS, Warrendale, PA, 1998, 119-124

S. J. Glass, J. R. Michael, M. J. Readey, S. I. Wright, D. P. Field, Characterization of Microstructure and Crack Propagation in Alumina Using Orientation Imaging Microscopy, *Proc. 1996 Ceramic Microstructures Conference*, to appear, 1997

Invited Presentations

C.C. Battaile, T.E. Buchheit, E.A. Holm, G.W. Wellman, M.K. Neilsen, Simulations of Microstructural Evolution in Deformed Polycrystals (Invited), Argonne Theory Institute, Argonne, IL, USA, August, 1999

V.R. Vedula, S.J. Glass, D.M. Saylor, G.S. Rohrer, W.C. Carter, Predicting microstructural level residual stresses and crack paths in ceramics (Invited poster), Gordon Research Conference, Solid State Studies in Ceramics, Holderness, NH, USA, June, 1999

E. A. Holm, Modeling Microstructure-Property Relationships (Invited), Michigan State University Physics Department Colloquium, Lansing, MI, USA, May, 1999

E. A. Holm, Modeling of Microstructure-Property Relationships (Invited), 1999 Spring Meeting of the Ohio Section of the APS, Flint, MI, USA, May, 1999

H. E. Fang, Multi-Level Modeling of Thermomechanical Fatigue in Solder Joints (Invited), Seminar at Univ. of Missouri, Columbia, MO, USA, March, 1999

V.R. Vedula and S.J. Glass, Residual stress predictions in alumina (Invited), CRC/NIST workshop: Microstructure-based Computational Methods for Reliability Prediction in Ceramics, Gaithersburg, MD, USA, 1999

Elizabeth A. Holm, Modeling of Microstructure-Property Relationships (Invited), Gordon Research Conference on Physical Metallurgy, Holderness, NH, USA, June, 1998

Elizabeth A. Holm, Corbett C. Battaile, Mark D. Rintoul, H. Eliot Fang, Applications of Grain Growth Modeling (Invited), Third International Conference on Grain Growth, Pittsburgh, PA, USA, June, 1998

H. E. Fang, Computational Modeling of Solder Joint Aging (Invited), ER/SSI Materials Group Meeting, ORNL, May 1998.

Elizabeth A. Holm, Computers in Materials Science: Processing, Performance, and Reliability Modeling (Invited), ASM International Peoria Chapter Meeting, Peoria, IL, USA, September, 1997

Elizabeth A. Holm, Applications of Mesoscale Materials Models at Sandia (Invited), Caterpillar Research Group Seminar, Peoria, IL, USA, September, 1997

H. E. Fang, M. K. Neilsen, E. A. Holm, Computational Modeling of Material Aging and Reliability (Invited), UI-Chicago seminar, Chicago, IL, USA, September, 1997

H. E. Fang, Computational Modeling of Thermomechanical Fatigue (TMF) of Solder Joint (Invited), Motorola Inc. Seminar, Albuquerque, NM, USA, September, 1997

E. A. Holm, Applications of Mesoscale Materials Models (Invited), American Ceramic Society Annual Meeting, Theory and Computational Modeling Symposium, Cincinnati, OH, USA, May, 1997

E. A. Holm, T. E. Buchheit, T. P. Swiler, Coupling Microstructural Simulation to Property Calculation (Invited), Symposium on Dynamics of Microstructure, University of Michigan, Ann Arbor, MI, USA, May, 1997

H. E. Fang, Computational Modeling of Material Aging and Reliability (Invited), UCSB Seminar, Santa Barbara, CA, USA, February, 1997

E. A. Holm, Boundary Energy and Mobility Effects in Polycrystalline Grain Growth (Invited), ASM/TMS Materials Week '96, Kinetically Determined Particle Shapes Symposium, Cincinnati, OH, USA, October, 1996

Contributed Presentations

T.E. Buchheit, G.W. Wellman, Evolution of a Flow Surface As-Predicted by a Polycrystal Plasticity Deformation Model, Materials Research Society Fall Meeting, Boston, MA, USA, December, 1999

V.R. Vedula, S.J. Glass, Residual stresses and cracking in alumina, Materials Research Society Fall Meeting, Boston, MA, USA, December, 1999

T.E. Buchheit, D.A. LaVan, G.W. Wellman, M.K. Neilsen, Comparison Between Simulation and Experiment of a Polycrystal Plasticity Deformation Model, TMS Fall Meeting, Cincinnati, OH, USA, November, 1999

Y.-L. Shen, W. Li, D. L. Sulsky, H. L. Schreyer, Localization of Plastic Deformation Along Grain Boundaries in a Hardening Material, ASME Mechanics and Materials Conference, Blacksburg, VA, USA, June, 1999

V.R. Vedula, S.J. Glass, W.C. Carter, S.A. Langer, Predicting microstructural level residual stresses in ceramics using object oriented finite element analysis (OOF), 101st American Ceramic Society Annual Meeting, Indianapolis, IN, USA, April, 1999

S.J. Glass, V.R. Vedula, D.M. Saylor, G.S. Rohrer, Application of electron backscattered diffraction (EBSD) and atomic force microscopy (AFM) to determine texture, microtexture, and grain boundary energies in ceramics, The 12th International Conference on Textures of Materials, Montreal, Qu, Canada, 1999

V.R. Vedula, S.J. Glass, D.M. Saylor, G.S. Rohrer, W.C. Carter, Predicting microstructural level residual stresses and crack paths in ceramics, The 12th International Conference on Textures of Materials, Montreal, Qu, Canada, 1999

C. C. Battaile, E. A. Holm, T. Buchheit, G. Wellman, M. Neilsen, Coupled Simulations of Mechanical Deformation and Microstructural Evolution Using Polycrystal Plasticity and Monte Carlo Potts Models, Fall 1998 Meeting of the Materials Research Society, Boston, MA, USA, December, 1998

H. E. Fang, E. A. Holm, Multi-Level Modeling of Thermomechanical Fatigue in Solder Joints, Tri-Laboratory Engineering Conference on Modeling and Simulation, Los Alamos, NM, USA, November, 1998

V. Vedula, S. J. Glass, E. A. Holm, Modeling Microstructure-Level Elastic Stresses in Alumina Using NIST's OOF and Sandia's JAS-3D Codes, NMACerS/ASM Annual Meeting, Albuquerque, NM, USA, October, 1998

Richard M. Fye, Fast Algorithm for Simulating Grain Growth Using the Potts Model, 1998 Conference on Computational Physics, Granada, Spain, September, 1998

C. C. Battaile and E. A. Holm, Evolution of 2D Potts Model Grain Microstructures from an Initial Hillert Size Distribution, Third International Conference on Grain Growth, Pittsburgh, PA, June 1998.

A. D. Rollett, E. A. Holm, The Link Between Kinetics and Configurational Statistics in Two Dimensional Grain Growth: Comparison of Theory and Simulation, Third International Conference on Grain Growth, Pittsburgh, PA, June 1998.

Richard M. Fye, Fast Algorithm for Potts Model Simulations of Grain Growth, DOE/AMS Workshop on Mathematical Aspects of Materials Science Modeling, Gatlinburg, TN, USA, April, 1998

Thomas E. Buchheit, Gerald W. Wellman, Michael K. Neilsen and Roy .J. Bourcier, 3-D deformation simulations of Polycrystalline FCC Metals, 2nd Biennial Tri-Laboratory Engineering Conference on Modeling and Simulation, Santa Fe, NM, USA, November, 1997

H. Eliot Fang, Victoria L. Porter, Richard M. Fye, and Elizabeth A. Holm, Multi-Level Modeling of Thermomechanical Fatigue in Solder Joints, 2nd Biennel Tri-Laboratory Engineering Conference on Modeling and Simulation, Los Alamos, NM, USA, November, 1997

H. Eliot Fang, unknown, SC97, San Jose, CA, USA, November, 1997

E. A. Holm, H. E. Fang, Minimum Energy Intergranular Crack Paths, ASM/TMS Materials Week '96, Fundamentals of Fracture and Deformation Symposium, Cincinnati, OH, USA, October, 1997

H. E. Fang, V. L. Porter, R. M. Fye, E. A. Holm, Simulation of Thermomechanical Fatigue in Solder Joints, 5th Joint Russian-American Conference on Computational Mathematics, Albuquerque, NM, USA, September, 1997

H. Eliot Fang, Victoria L. Porter, Richard M. Fye, and Elizabeth A. Holm, Simulation of Thermomechanical Fatigue in Solder Joints, 5th Joint Conference on Computational Mathematics, Albuquerque, NM, USA, September, 1997

E. A. Holm, H. E. Fang, Intergranular Crack Surfaces of Minimum Energy, American Ceramic Society Annual Meeting, Theory and Computational Modeling Symposium, Cincinnati, OH, USA, May, 1997

T. E. Buchheit, R. J. Bourcier, M. K. Neilsen, G. W. Wellman, Deformation Simulations of Three-Dimensional Polycrystals, Computational Materials Science at the Mesoscale Symposium, MRS Spring Meeting, San Francisco, CA, USA, April, 1997

S. J. Glass, Reliability and Lifetime Prediction Needs and Challenges for Ceramic Components in the Nuclear Weapon Stockpile, U. of Houston Reliability Workshop, Houston, Mechanical Engineering Dept., Houston, TX, USA, February, 1997

S. J. Glass, J. R. Michael, M. J. Readey, S. I. Wright, D. P. Field, Characterization of Microstructure and Crack Propagation in Alumina Using Orientation Imaging Microscopy, 1996 Ceramic Microstructures Conference, Berkeley, CA, USA, June, 1996

International Workshop

H. E. Fang, E. A. Holm, A Focused Workshop on Computational Approaches to Linking Microstructure and Mechanical Response, April, 1999

Figures

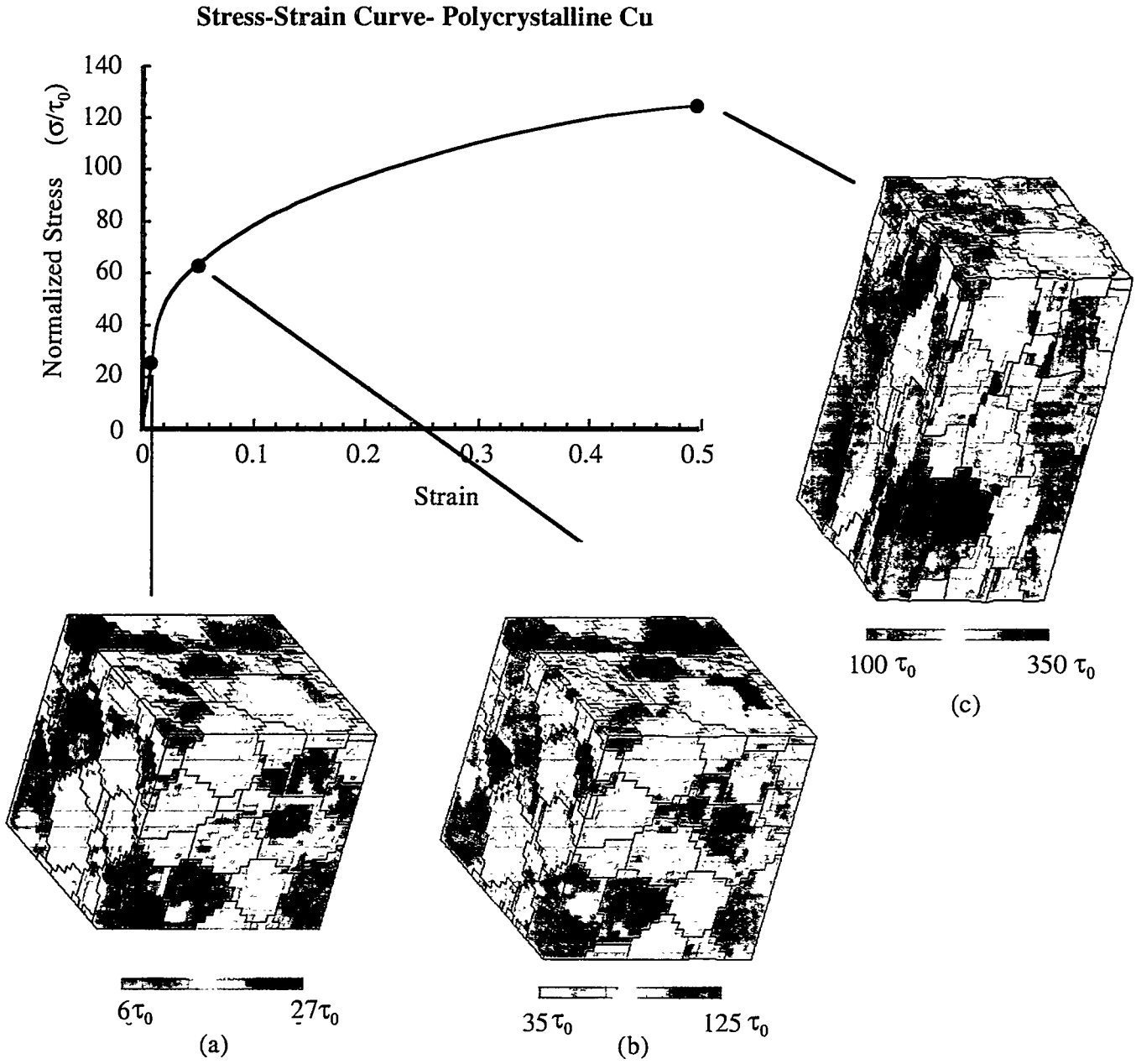

Figure 1. Simulated tensile deformation response of a Copper polycrystal using the microstructure mechanics model with Bassani-type anisotropic work hardening. Distribution of Von Mises stress is illustrated at (a) 0.5%, (b) 5% and (c) 50% strain.

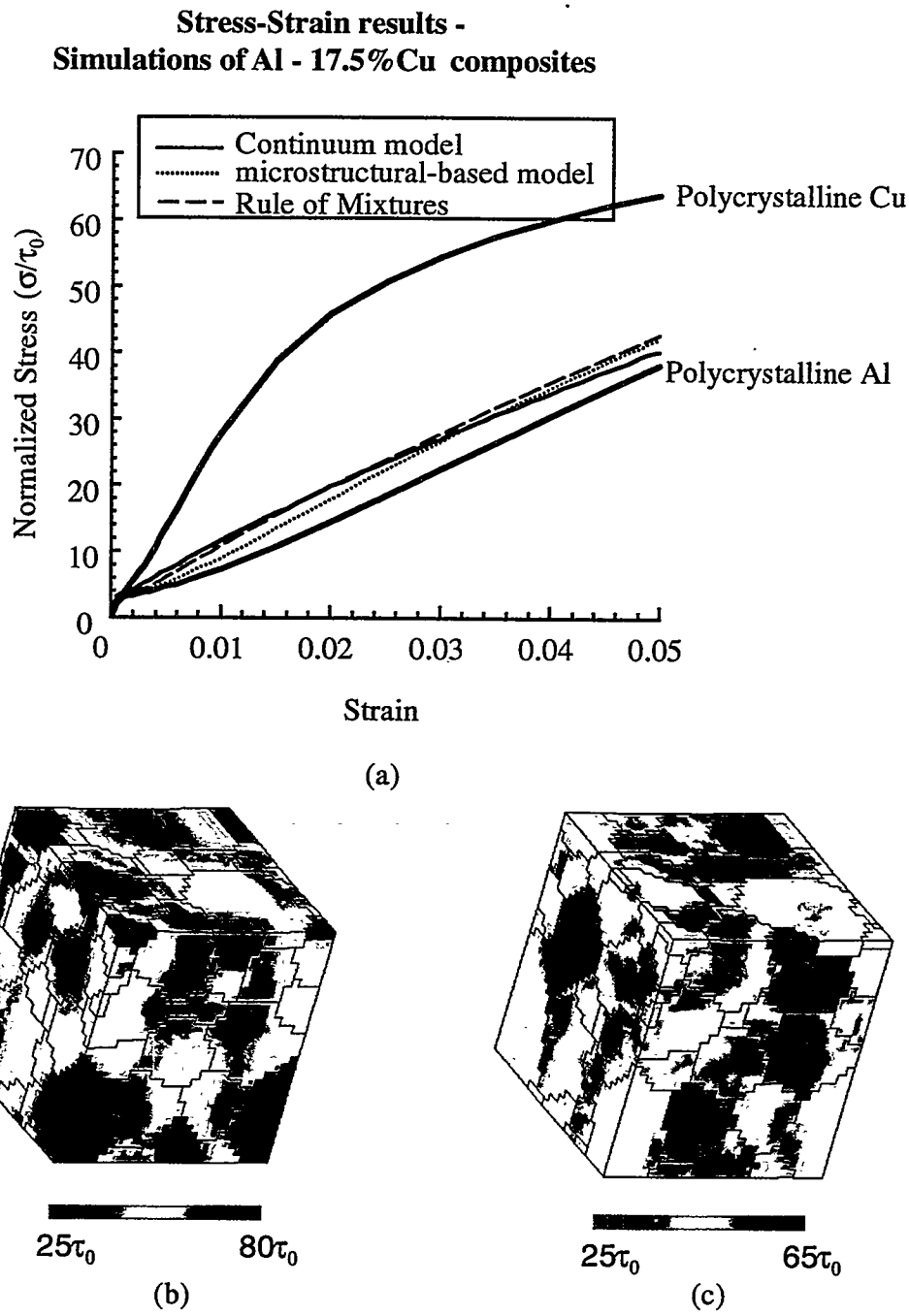

Figure 2. (a) Predicted Stress-Strain response of a hypothetical Al-17.5%Cu two-phase material using microstructure mechanics model and a continuum plasticity model. The response of each phase is also illustrated. (b) Von Mises distribution in two-phase continuum, the copper phase is red. (c) Von Mises distribution in two-phase polycrystal.

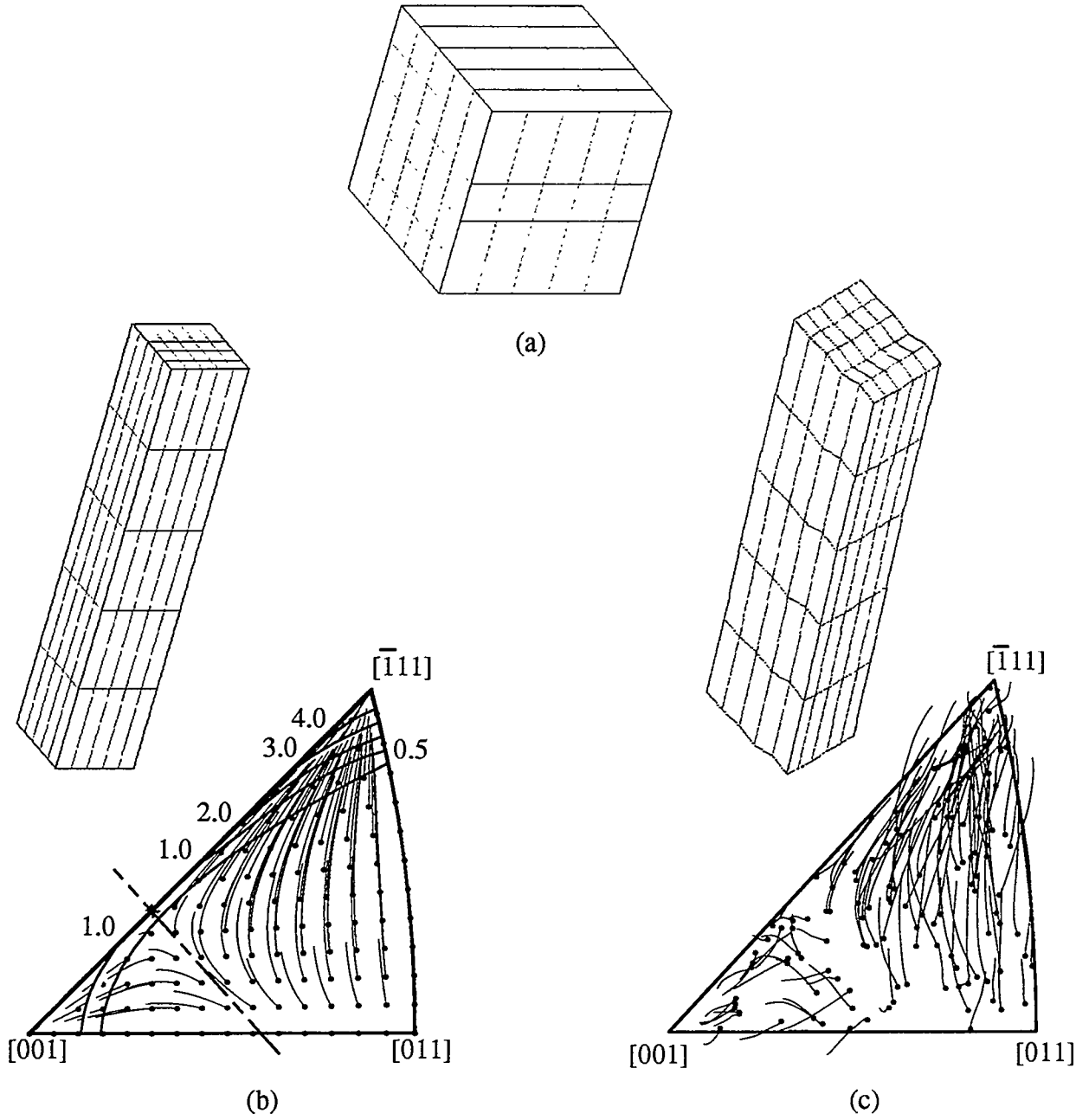

Figure 3. (a) 125 grain polycrystal in JAS-3D, 1 grain equals 1 finite element, (b) upper-bound isochoric deformation solution with rotations of a periodic distribution of grains tracked to 50% strain and compared with experimental data contours on an inverse pole figure, (c) JAS-3D finite element solution to isochoric deformation condition with rotations of each randomly oriented grain tracked to 50% strain on an inverse pole figure.

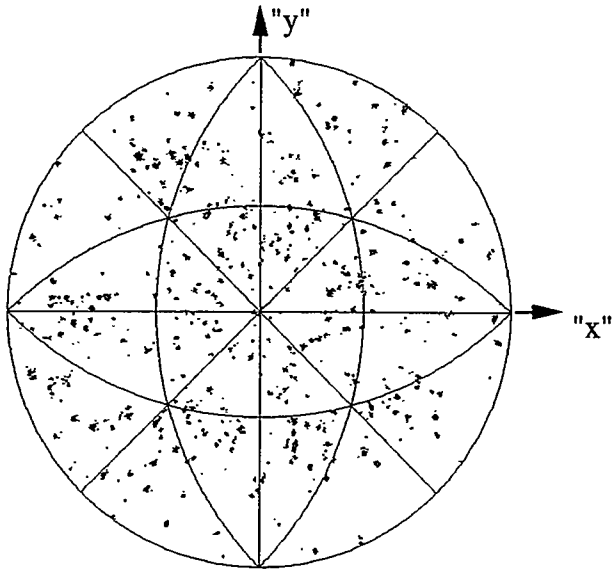

(a)

(b)

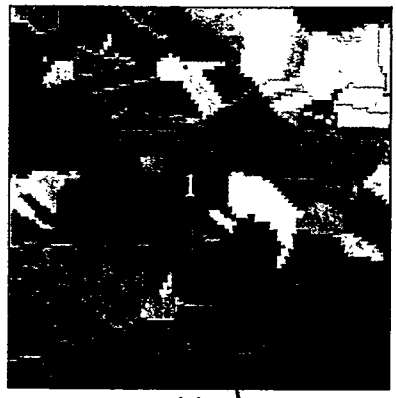

(c)

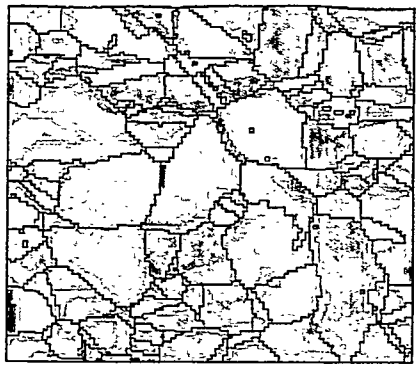

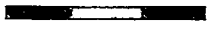

0° 10°

(d)

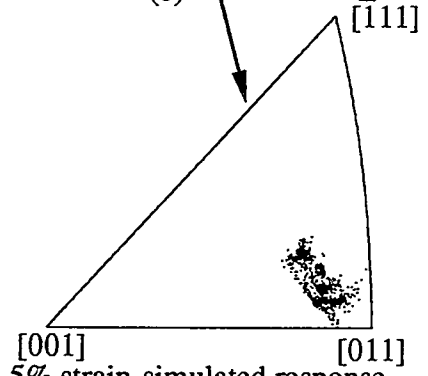

5% strain-simulated response
5% strain-experimental response
10% strain-simulated response

(e)

Figure 4. (a) <100> pole figure of as-collected OIM data. (b) 200 μm x 200 μm image of as-collected OIM data. (c) OIM data modified for microstructural deformation simulation. (d) simulated misorientations relative to original grain orientation after 10% strain on surface of a tension specimen. (e) inverse pole figure comparing experimental and simulated subgrain rotations for grain labeled "1".

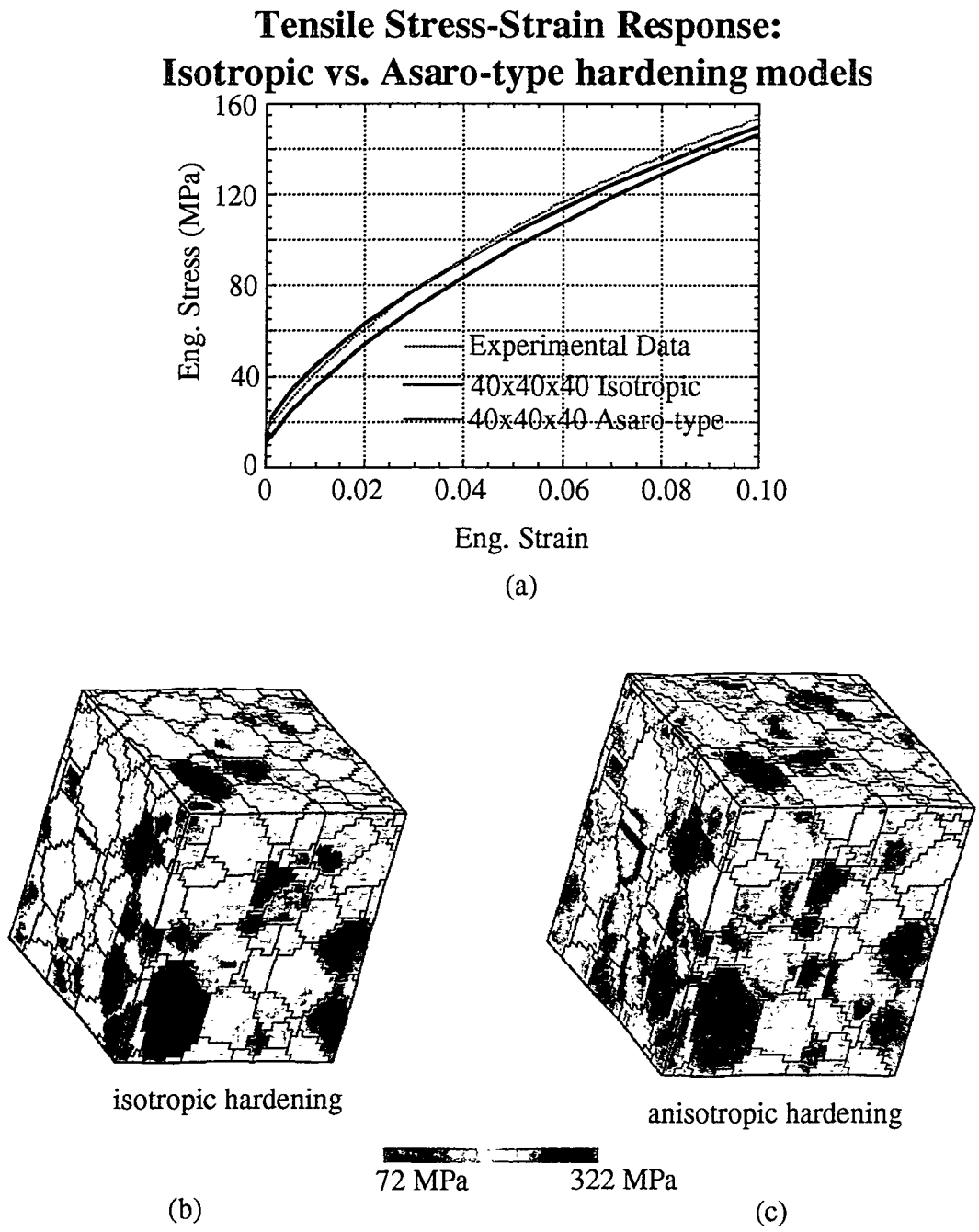

Figure 5. (a) A comparison of tensile stress-strain curves generated from an Asaro-type anisotropic hardening model, a Sandia developed isotropic hardening model and experimental data. (b) Von-Mises stress distribution in a polycrystal plasticity simulation using isotropic hardening model. (c) Von-Mises stress distribution in a polycrystal plasticity simulation using Asaro-type anisotropic hardening model.

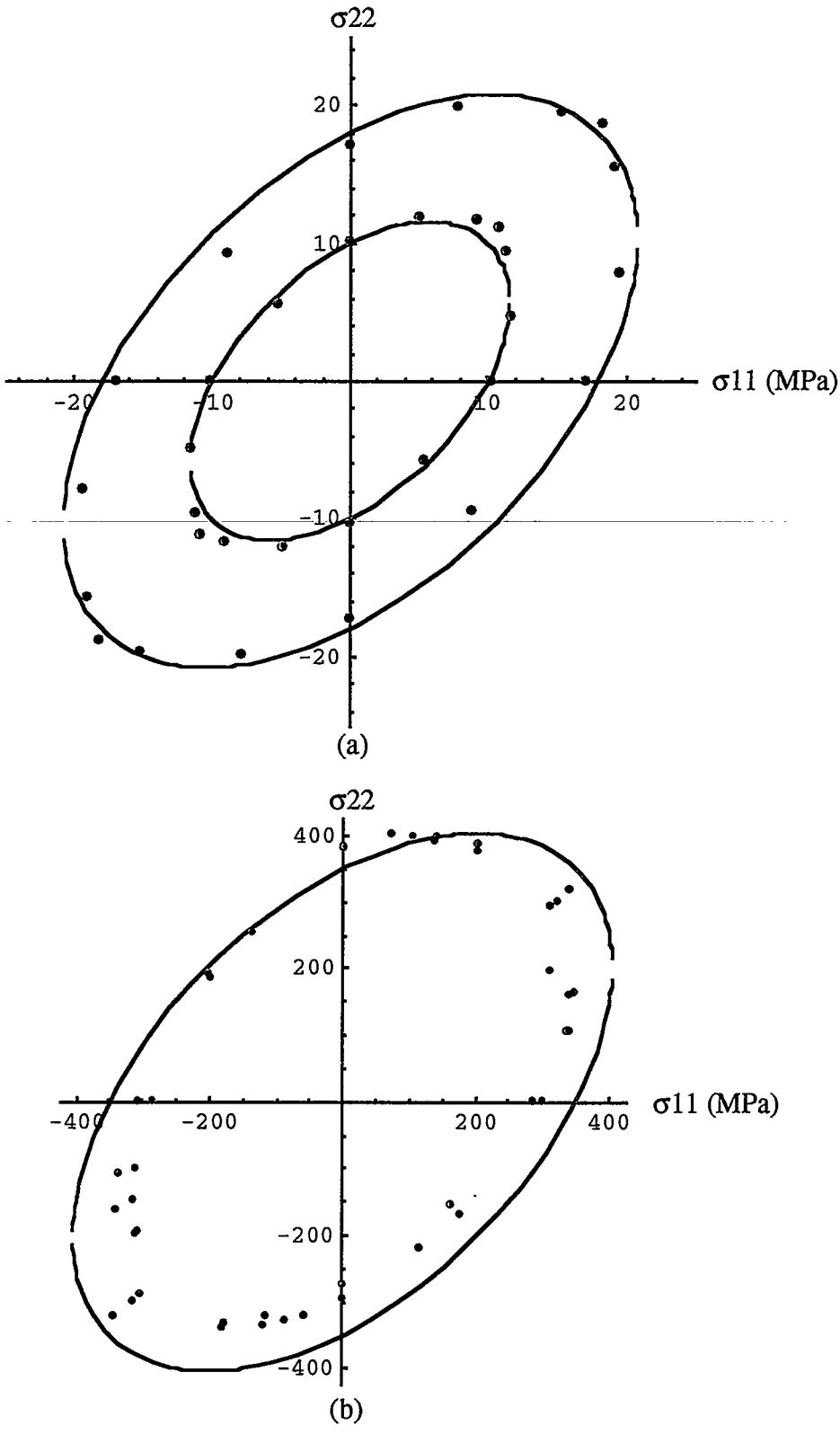

Figure 6. Yield data predictions for polycrystal plasticity simulations of 200 grains using Isotropic(Blue) and Asaro (Red) copper work hardening models at (a) 0% strain and (b) 50% strain.

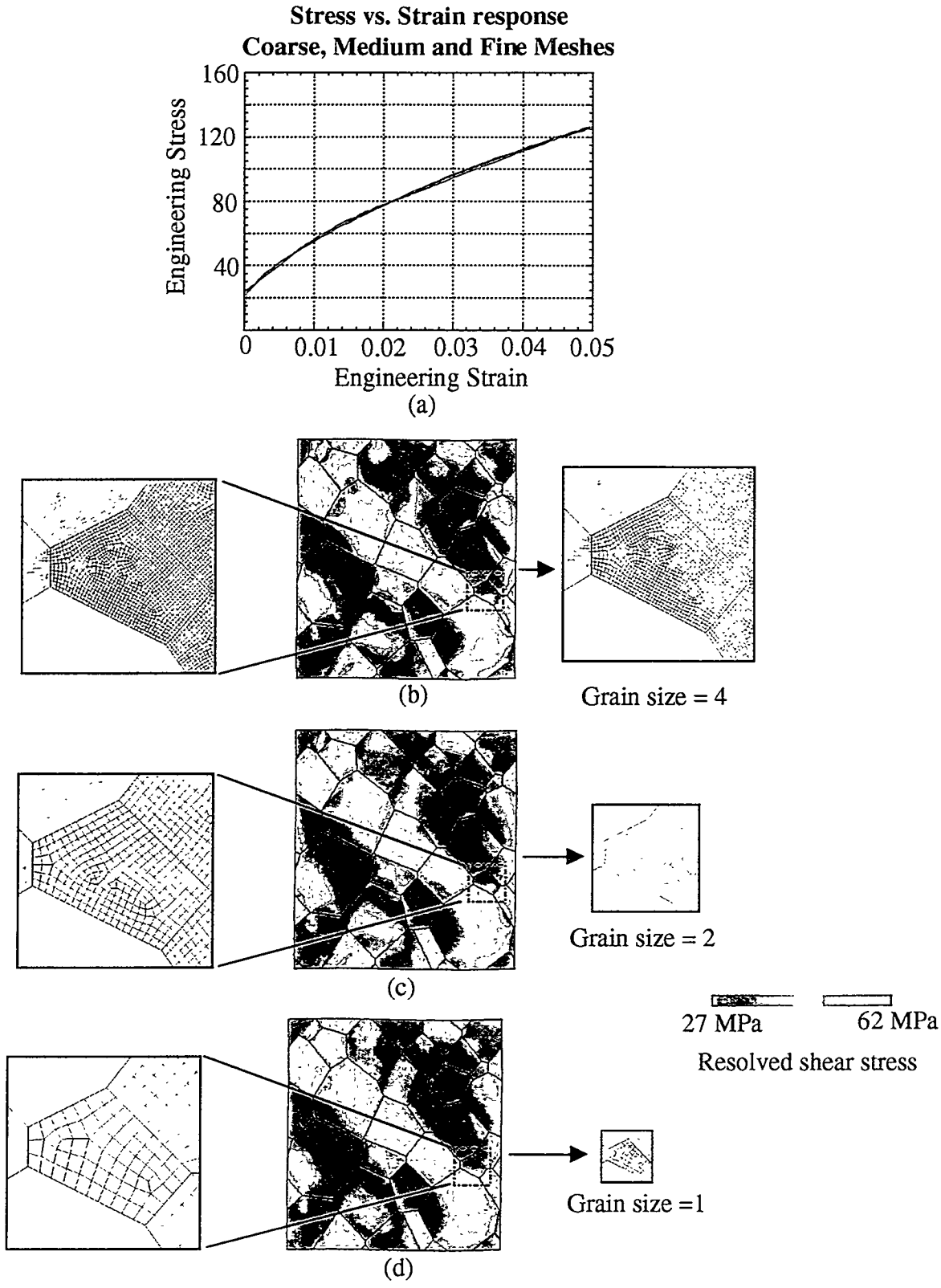

Figure 7. (a) Tensile stress strain response for polycrystal plasticity simulations at 3 different mesh densities. (b-d) Resolved shear stress distribution and grain size relationship for (b) fine scale, (c) medium scale, and (d) coarse scale mesh densities.

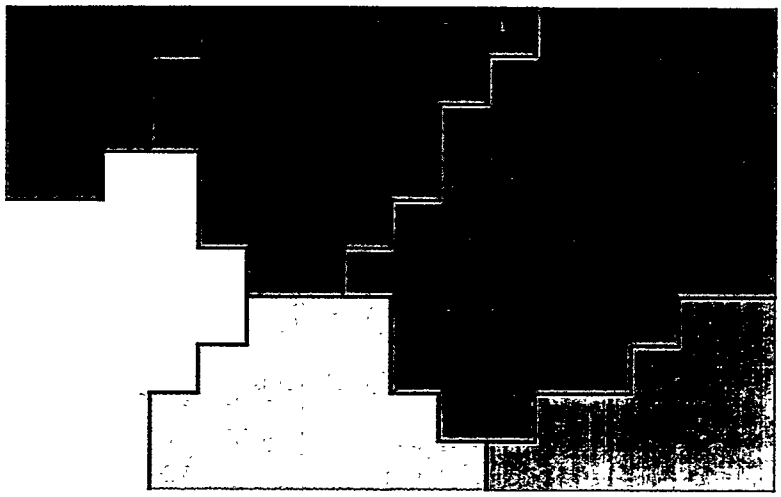

Figure 8. Schematic of a digitized Potts model microstructure. Different colors represent different pixel values, and black lines are grain boundaries.

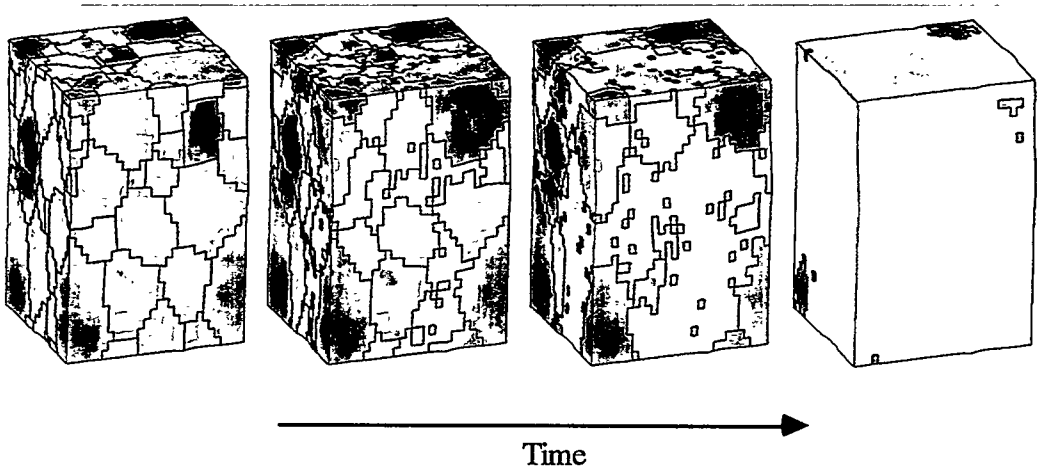

Figure 9. Grain growth in a Cu polycrystal elongated 30%. The colors indicate values of stored plastic energy (see equation 22) where blue is low and red is high.

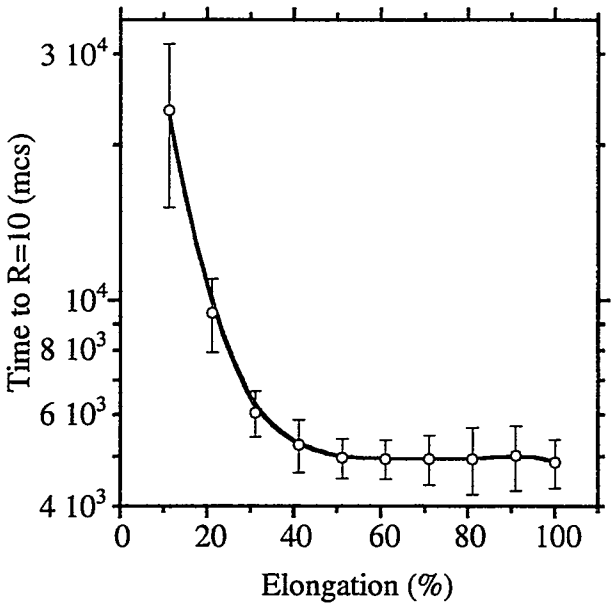

Figure 10. Grain growth rate (i.e., Monte Carlo time to reach an average grain size of 10 voxels) as a function of deformation. Error bars correspond to standard deviations over forty grain growth simulations.

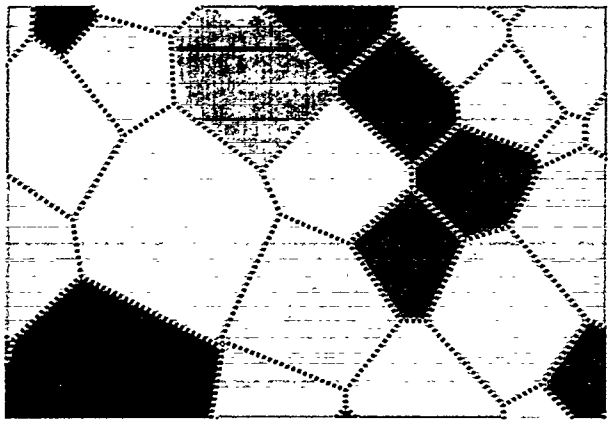

Figure 11. Schematic of a front tracking microstructure. Different colors represent different grains, and black dots are the boundary points used in the front tracking simulation (see text).

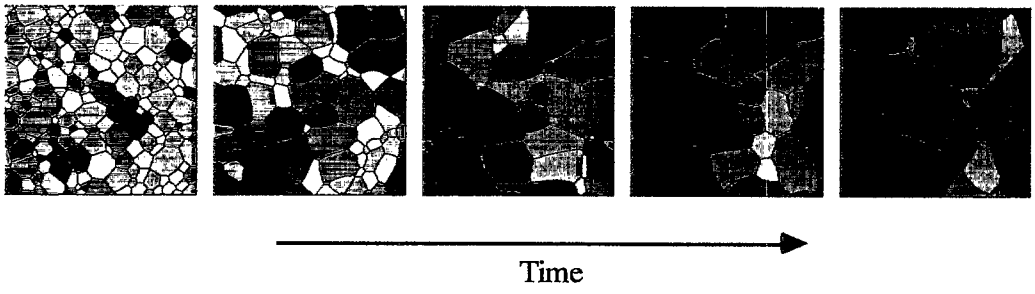

Figure 12. Grain growth in a Cu polycrystal elongated 1%. The colors indicate values of stored elastic energy (see equation 26) where blue is low and red is high.

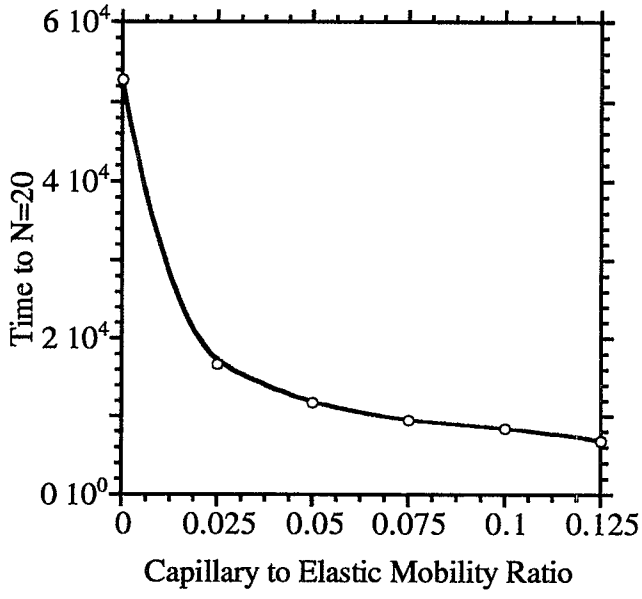

Figure 13. Grain growth rate (i.e., time to reach 20 grains) as a function of the ratio between the capillary and elastic mobility ratio, $M_\sigma : M_\kappa$ (see equation 25).

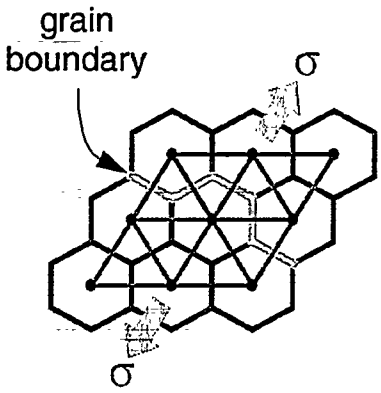

Figure 14.A GLAD model on a 2D triangular lattice.

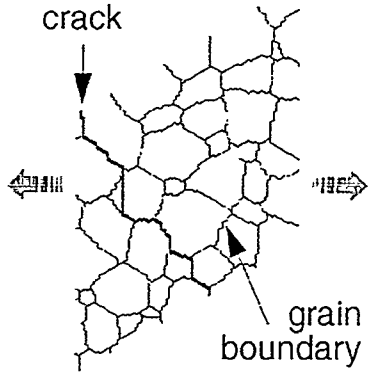

Figure 15.GLAD results of mixed inter- and intragranular cracking

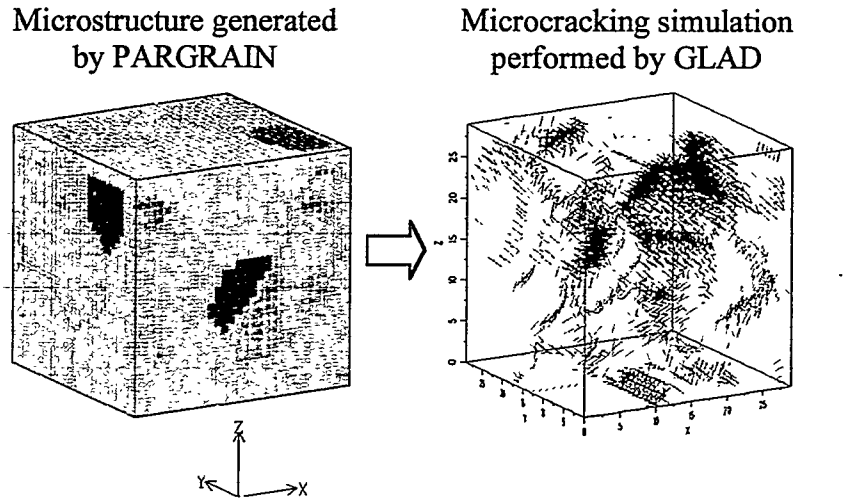

Figure 16. 3D GLAD simulation of anisotropic-thermal-expansion induced microcracking.

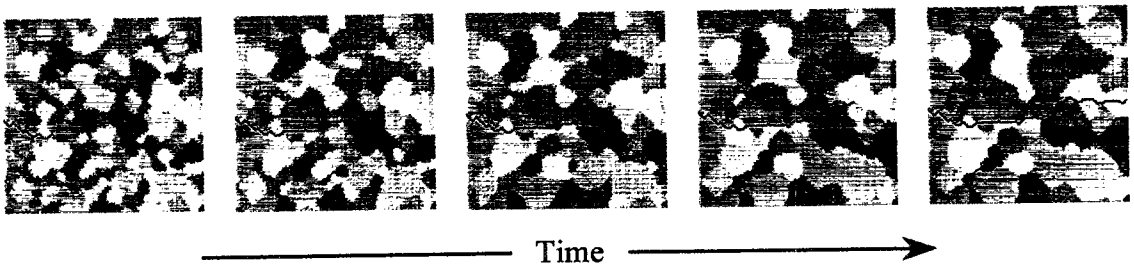

Figure 17.Coupled PARGRAIN/GLAD simulation of crack propagation in an evolving microstructure.

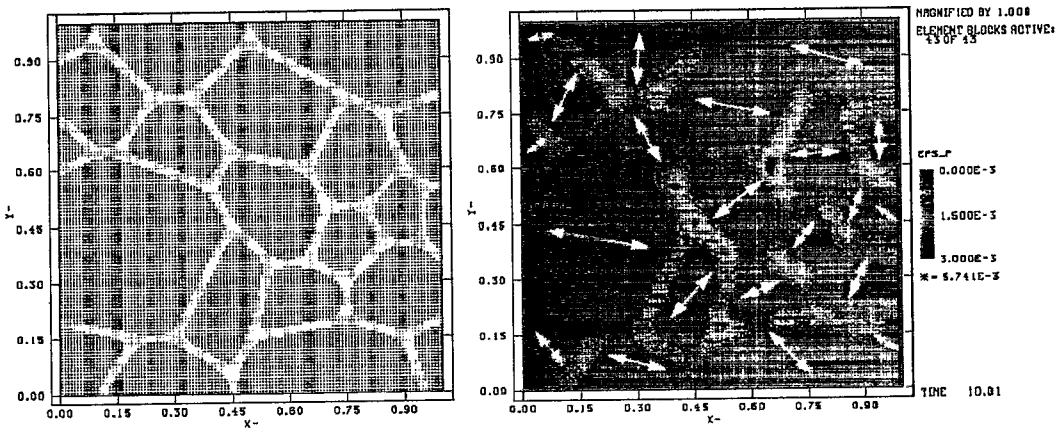

(a) (b)

Figure 18. 2D MPM simulation of anisotropic-thermal-expansion induced microcracking.

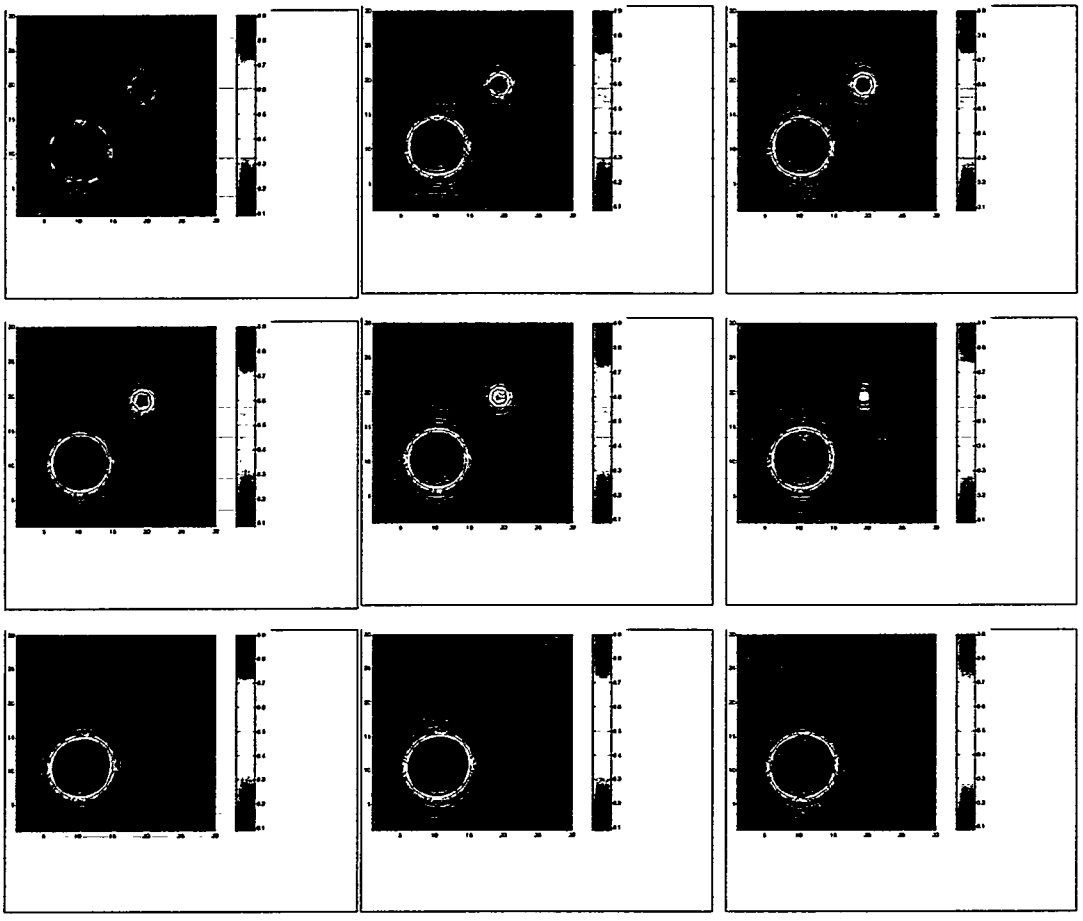

Figure 19.MPM simulation of microstructural evolution: interaction of two inclusions initially far apart.

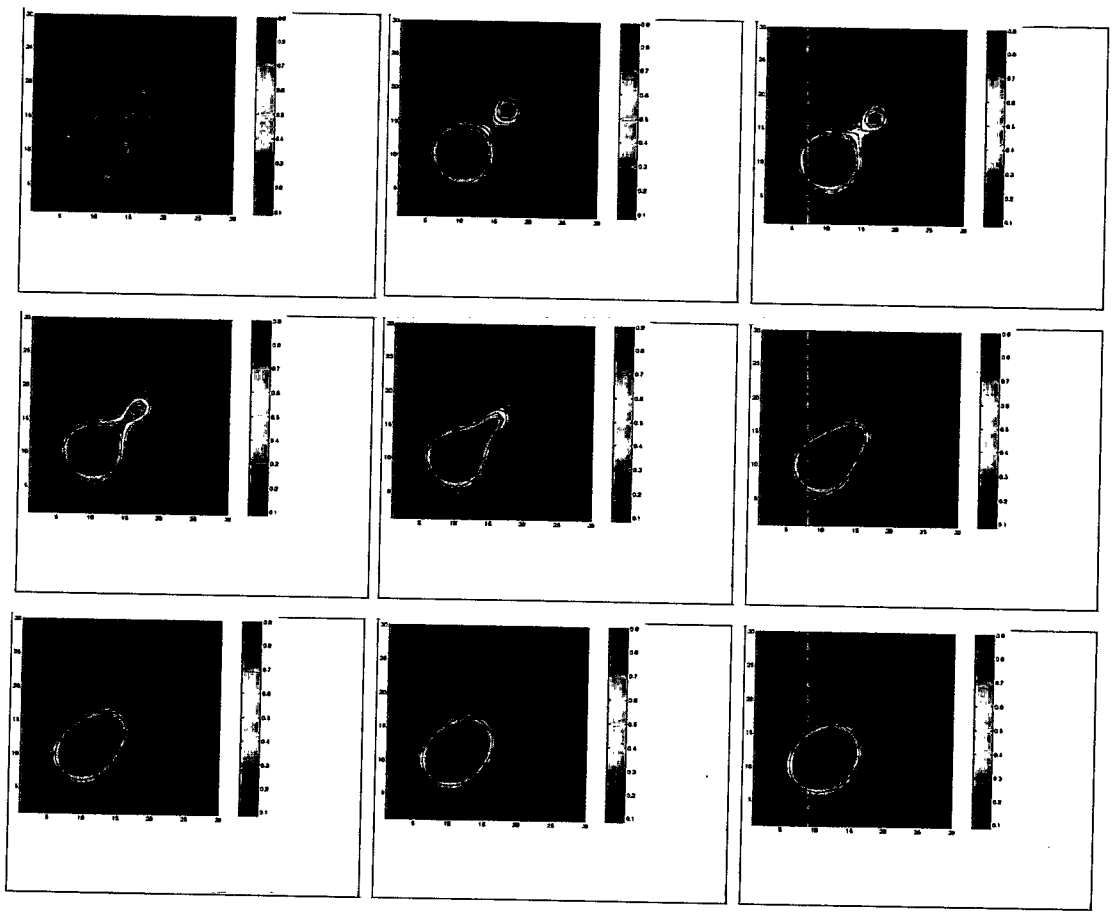

Figure 20.MPM simulation of microstructural evolution: interaction of two inclusions initially close to each other.

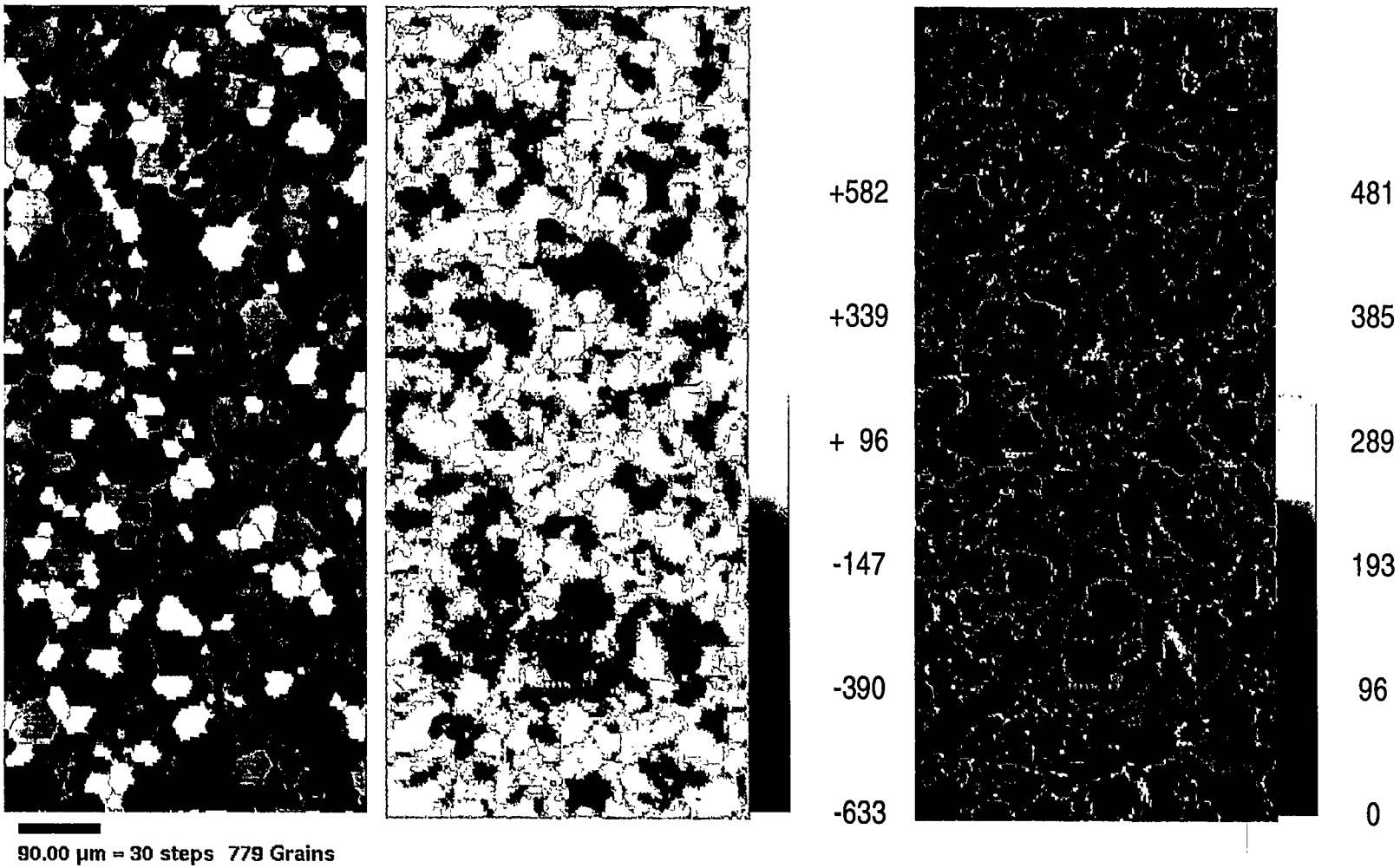

Figure 21. Residual stress distribution in alumina when ΔT=-1500°C. (a) OIM image showing different grains, (b) Stress Invariant 1 ($\sigma_{11}+\sigma_{22}$) in MPa, and (c) Maximum Principal Stress (σ_{11}) in MPa.

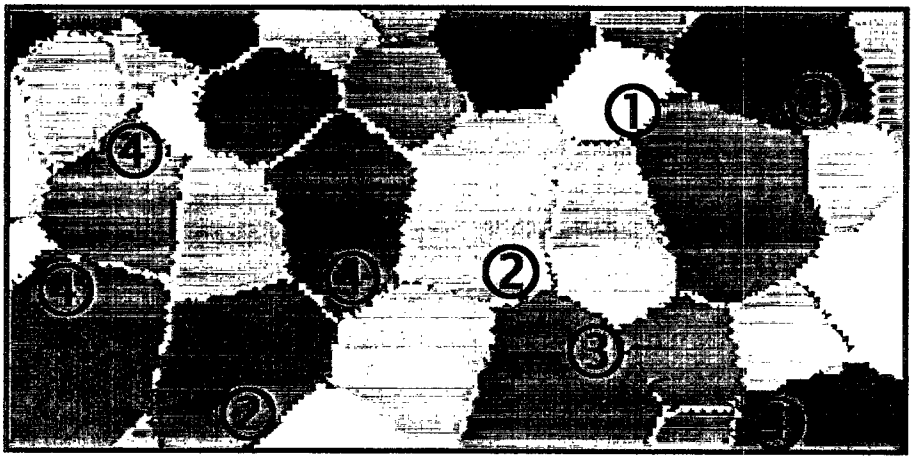

Figure 22. Crack initiation and propagation in alumina with increasing temperature difference. ① corresponds to -1160, ② to -1500, ③ to -1700, and ④ to -1900°C. Dark elements are fractured.

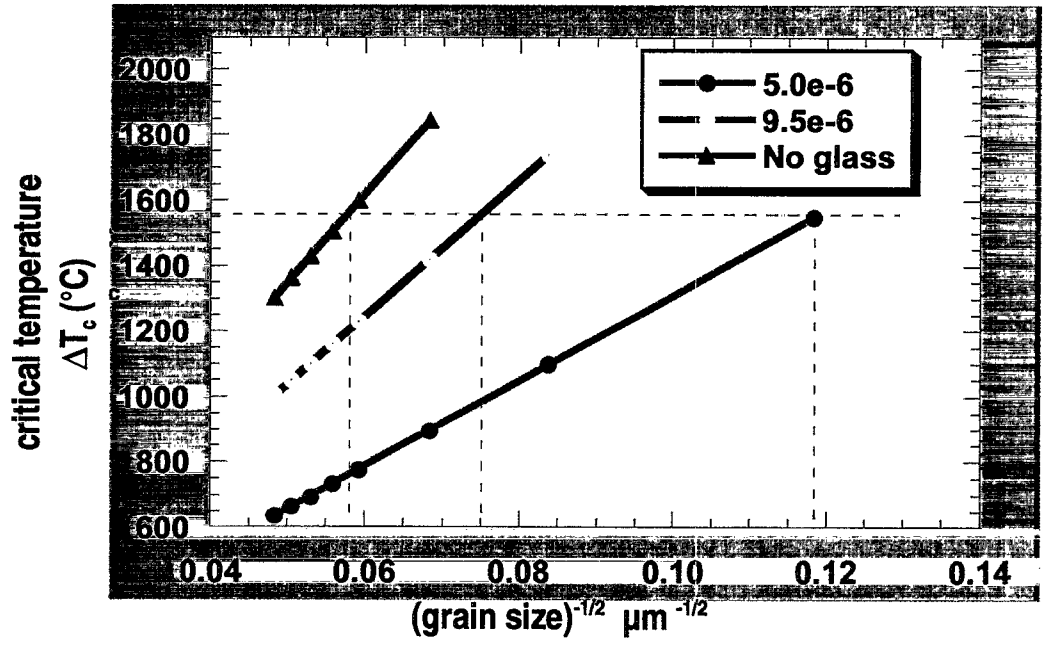

Figure 23. Critical temperature difference vs. grain size in alumina for two different grain boundary properties (α=9.5x10^{-6} and 5x10^{-6} /°C) and for boundaries with no glassy phase.

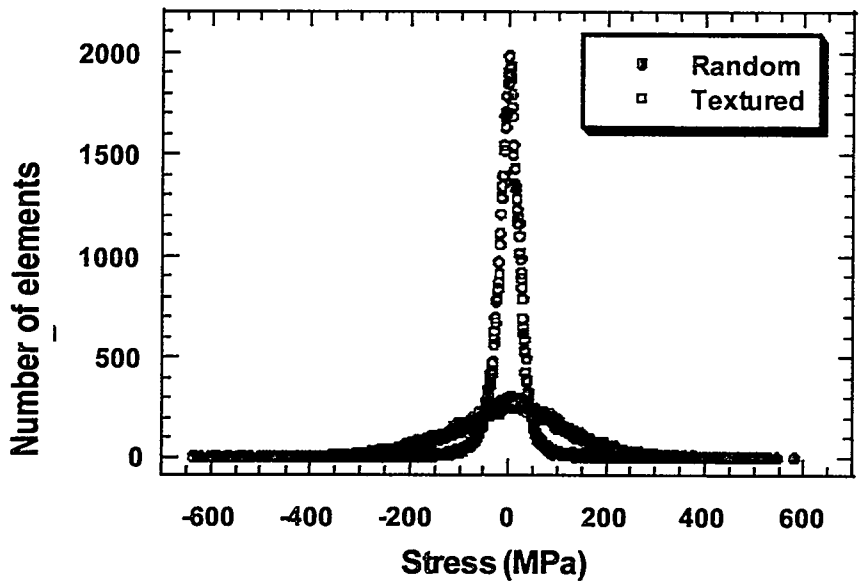

Figure 24. Residual stress distribution in textured and randomly oriented samples showing Number of elements versus Stress (Stress Invariant 1).

Copies	MS	Names	Org.
1		Prof. Deborah Sulsky University of New Mexico Albuquerque. NM USA	
1		Prof. Yu-LinShen University of New Mexico Albuquerque, NM USA	
1		Prof. H. Buck Schreyer University of New Mexico Albuquerque, NM USA	
1	1435	A Kay hays	1800
1	1434	Julia M. Phillips	1802
1	0367	Mark F. Smith	1833
1	0367	Geraln A. Knorovsky	1833
1	1411	H. Eliot Fang	1834
3	1411	Elizabeth A. Holm	1834
1	1411	Corbette C. Battaile	1834
1	0367	Richard Salzbrenner	1835
1	0333	Thomas E. Buchheit	1835
1	1411	Duane Dimos	1843
1	1411	Venkata Vedula	1843
1	0367	Jill S. Glass	1843
1	0321	William Camp	9200
1	1111	Mark D. Rintoul	9225
1	0841	Paul Hommert	9100
1	0847	Harold Morgan	9123
1	0847	Michael K. Neilsen	9123
1	0847	Gerald W. Wellman	9123

1	9018	Central Technical Files	8940-2
2	0899	Technical Library	9616
1	0612	Review and Approval Desk For DOE/OSTI	9612